PURDUE UNIVERSITY
GRADUATE SCHOOL
Thesis/Dissertation Acceptance

This is to certify that the thesis/dissertation prepared

By Amruth Bhargav

Entitled

Development of Novel Cathodes for High Energy Density Lithium Batteries

For the degree of Master of Science in Mechanical Engineering

Is approved by the final examining committee:

Yongzhu Fu
Chair

Likun Zhu

Jing Zhang

To the best of my knowledge and as understood by the student in the Thesis/Dissertation Agreement, Publication Delay, and Certification Disclaimer (Graduate School Form 32), this thesis/dissertation adheres to the provisions of Purdue University's "Policy of Integrity in Research" and the use of copyright material.

Approved by Major Professor(s): Yongzhu Fu

Approved by: Sohel Anwar 4/22/2016

Head of the Departmental Graduate Program Date

DEVELOPMENT OF NOVEL CATHODES FOR HIGH ENERGY DENSITY LITHIUM BATTERIES

A Thesis

Submitted to the Faculty

of

Purdue University

by

Amruth Bhargav

In Partial Fulfillment of the

Requirements for the Degree

of

Master of Science in Mechanical Engineering

May 2016

Purdue University

Indianapolis, Indiana

To the almighty and my parents

ACKNOWLEDGMENTS

I would like to thank my parents for their unconditional love and unrelenting support for my endeavors. Their guidance and kind words has helped me always.

I would like to express my sincere gratitude to my advisor Dr. Yongzhu Fu for the continuous support of my research, for his patience, motivation, enthusiasm, advice and immense knowledge. His timely guidance and training helped me carry out my research in an organized and professional way. I could not have imagined having a better advisor and mentor for my graduate study.

I thank my fellow labmates : Yi Cui and Min Wu for their invaluable support, engrossing discussions and the best atmosphere to work in. My sincere thanks also goes to lab members of Dr. Jian Xie : Dr. Le Xin, Fan Yang, Dr. Yadong Liu and Dr. Zhefei for their assistance.

TABLE OF CONTENTS

LIST OF FIGURES

Figure Page

Figure Page

ABSTRACT

Bhargav, Amruth. M.S.M.E, Purdue University, May 2016. Development of Novel Cathodes for High Energy Density Lithium Batteries. Major Professor: Yongzhu Fu.

Lithium based batteries have become ubiquitous with our everyday life. They have propelled a generation of smart personal electronics and electric transport. Their use is now percolating to various fields as a source of energy to facilitate the operation of devices from nanoscale to mega scale. This need for a portable energy source has led to tremendous scientific interest in this field to develop electrochemical devices like batteries with higher capacities, longer cycle life and increased safety at a low cost.

To this end, the research presented in this thesis focuses on two emerging and promising technologies called lithium-oxygen (Li-O_2) and lithium-sulfur (Li-S) batteries. These batteries can offer an order of magnitude higher capacities through cheap, environmentally safe and abundant elements namely oxygen and sulfur.

The first work introduces the concept of closed system lithium-oxygen batteries wherein the cell contains the discharge product of Li-O_2 batteries namely, lithium peroxide (Li_2O_2) as the starting active material. The reversibility of this system is analyzed along with its rate performance. The possible use of such a cathode in a full cell is explored. Also, this concept is used to verify if all the lithium can be extracted from the cathode in the first charge.

In the following work, lithium peroxide is chemically synthesized and deposited in a carbon nanofiber matrix. This forms a free standing cathode that shows high reversibility. It can be cycled up to 20 times and while using capacity control protocol, a cycle life of 50 is obtained. The cause of cell degradation and failure is also analyzed. In the work on full cell lithium-sulfur system, a novel electrolyte is developed that can support reversible lithium insertion and extraction from a graphite anode. A

method to deposit solid lithium polysulfide is developed for the cathode. Coupling a lithiated graphite anode with the cathode using the new electrolyte yields a full cell whose performance is characterized and its post-mortem analysis yields information on the cell failure mechanism.

Although still in their developmental stages, Li-O_2 and Li-S batteries hold great promise to be the next generation of lithium batteries and these studies make a fundamental contribution towards novel cathode and cell architecture for these batteries.

1. INTRODUCTION

Mankind is depleting non-renewable sources of energy at an ever increasing rate. This, along with the booming portable electronics industry and the impetus to make long range electric vehicles has placed an unprecedented high demand for electrochemical energy storage devices. The commercialization and advancement of lithium-ion (Li-ion) batteries was a major step in coping with this demand. Higher specific energy in the range of 100-250 $Wh\ kg^{-1}$ offered by Li-ion batteries placed it as a better candidate than other aqueous electrolyte-based battery chemistries for the aforementioned uses.[1] Despite rapid advancement in recent years to develop high voltage cathodes (e.g., $LiMn_{1.5}Ni_{0.5}O_4$) to push the specific energy limit, the stability window of organic electrolytes in the current Li-ion batteries seems to be the barrier in achieving this goal.[2] Beyond Li-ion technologies such as Li-O_2 and Li-S batteries have garnered much scientific interest in recent years as they have high capacities albeit operating at lower voltages, providing specific energies several-fold more than current Li-ion batteries.[3]

Li-O2 batteries use the lightweight and abundant oxygen reacting with incoming lithium ion at a porous carbon cathode giving a high capacity. The cell discharge reaction is given by:

$$O_2 + 2Li^+ + 2e^- \longrightarrow Li_2O_2 \tag{1.1}$$

Thus, based on the capacity of the discharge compound, Li_2O_2, such cells have a theoretical capacity of 1,168 $mAh\ g^{-1}$. The overall standard potential for this type of cell is 2.96 V, yielding a specific energy of 3,458 $Wh\ kg^{-1}$. Such high specific energy densities make them promising for use in electric vehicles.[4]

Another promising alternative is the lithium-sulfur battery (Li-S). In this battery, elemental sulfur undergoes a 2 electron reaction and combines with lithium to yield

lithium sulfide. This process occurs through a number of intermediate steps involving lithium polysulfides Li_2S_x (8 X 2). The overall reaction during the discharge process is given below:

$$S + 2Li^+ + 2e^- \longrightarrow Li_2S \tag{1.2}$$

Therefore, the cell can also function through the introduction of a solid species of the lithium polysulfide (Li_2S_6) as developed in this work.

A brief introduction to the motivation for work contained in each chapter is listed in the beginning section of each chapter.

2. LITHIUM PEROXIDE-CARBON COMPOSITE CATHODE

2.1 Introduction

Current Li-O_2 batteries are based on an "open system" design. These cells typically use Swagelok-type configuration which has a porous carbon cathode.[5] Thus, these cells "breathe" oxygen during discharge and convert it to Li_2O_2, and regenerate oxygen during charging. The major problems with this system are severe electrolyte decomposition, cathode instability leading to the formation of Li_2CO_3 among other decomposition products,[6] and dendrite formation on the lithium metal anode.[7] The lithium metal anodes are reactive and suffer from low Coulombic efficiency in the lithium deposition and stripping process. From a practical implementation point of view, open system Li-O_2 batteries have several drawbacks. They use pure O_2, which means that, practical systems would need to carry O_2 cylinder on board or use devices like air scrubbers to purify and filter atmospheric air for use. Also, the electrochemistry in these batteries is very sensitive to the O_2 quality and presence of impurities like CO_2 and H_2O.[8,9] Thus, these ancillary systems would reduce the specific energy output and also increase operating and maintenance costs. Using the open system also needs the management of electrolyte evaporation. Safety concerns regarding operating lithium metal anodes and carrying oxygen also exist. Open systems use carbon cathodes and hence cannot account for the exact amount of Li_2O_2 present at any given point of time. There is inconsistent reporting of system performance metrics in the field due to sensitivity of electrochemistry and the lack of standardization in spite of similar cell designs.[8] In addition, the capacity limited cycling method is widely used, which cannot bring out the latent instabilities of some open systems.[10] Closed system Li-O_2 batteries start with Li_2O_2 cathodes which could eliminate some of the issues with open systems. To the best of our knowl-

edge, there is no systematic study yet. Li_2O_2 embedded cathodes have been used to study the first charge characteristics in which specific capacities of first charges were reported; however, no discharge and cycling performance have been reported.[11,12]

In this study we present a binder-free cathode configuration in a closed system which starts with the discharge product Li_2O_2. As O_2 gas is generated during the charge process, it eliminates the need for pure O_2 cylinders or purification systems. This concept also explores the idea of storing O_2 produced during charge within the cell to enable reuse during discharge. A high first discharge capacity with high cycle efficiency is demonstrated based solely on Li_2O_2 rechargeability. It also explores the possibility of using a non-lithium metal, i.e., graphite anode, in conjunction with such cathode configuration to realize a full cell that could be a step towards practical implementation of Li-O_2 batteries.

2.2 Experimental

2.2.1 Li_2O_2-Nano24 Composite and Binder-Free Carbon Current Collector

Lithium peroxide (Li_2O_2, 95%, Arcos organics) and Nano24, a nanographite with 350 $m^2\ g^{-1}$ surface area (Asbury carbons) in 1:1 weight ratio was ground together for 15 minutes with a mortar and pestle to form the Li_2O_2-Nano24 composite in an Argon-filled glove box (MBraun). Two types of binder-free carbon current collectors were used. Commercial multi-walled carbon nanotube (MWCNT) paper called buckypaper (Buckeye Composites) was cut into $\sim$ 1 cm^2 discs (weighing $\sim$ 2 mg) and dried overnight at 100° C under vacuum before use. Toray carbon paper (Fuel Cell Earth) was cut into similar 1 cm^2 discs (weighing $\sim$ 12.4 mg) and was used in cells made for *ex situ* characterization owing to its better mechanical strength. It was also used as graphitic anode in the full cell with about 50% of its weight assumed to be graphitic carbon.[13]

2.2.2 Electrolytes

The electrolytes used in this study were 1 M lithium trifluoromethanesulfonate ($LiCF_3SO_3$, 98%, Arcos organics) in 1,2-dimethoxyethane (DME, 99+%, stabilized with BHT, Arcos organics) which is the main electrolyte in this work and was replaced in situations wherein it does not support the required performance, 0.5 M lithium nitrate ($LiNO_3$, 99+% , Arcos organics) in DME for high rate performance testing. Full cell analysis used liquid carbonate electrolyte (Novolyte, 1 M $LiPF_6$ in ethylene carbonate/diethyl carbonate (EC/DEC, 1:1 v/v)).

2.2.3 Cell Assembly

A CR2032 coin cell was assembled in the glove box with a weighed quantity of the Li_2O_2-Nano24 composite on a buckypaper or carbon paper disc. The powder was then spread as evenly as possible using a spatula. To this 20 L of electrolyte was added to make the power wet and adhere to the current collector. Then, another buckypaper or carbon paper disc was placed on top and 40 μL of electrolyte was added. This was enough to keep the entire cathode completely wetted. A Celgard 2400 separator was placed on the cathode, additional 20 μL of the electrolyte was added and lithium metal foil with nickel-foam current collector was placed to complete the cell. In case of full cells, the Li metal foil was replaced with carbon paper at the anode side. Finally, the cells were crimped for electrochemical testing.

2.2.4 Characterization

For *ex situ* characterization, cells were made with carbon paper- Li_2O_2 composite sandwich configuration and electrochemically tested as required. The cell was then opened; the cathode was carefully extracted and thoroughly washed with DME and dried in the glove box atmosphere. It was then sealed in a suitable container under Argon and transferred carefully to the testing equipment. Scanning electron

microscopy (SEM) was performed with a JEOL JSM-7800F field emission scanning electron microscope equipped with energy-dispersive X-ray spectroscopy (EDS). Powder X-ray diffraction (XRD) was performed with the top carbon paper of the sandwich removed and the sample protected in the sample holder by Kapton film. This sample was prepared under dry nitrogen atmosphere. Data were collected on a PANalytical Empyrean X-ray diffractometer equipped with Cu Kα radiation source for 2θ between 20° and 80° at a scan rate of $1°min^{-1}$. The XRD pattern of the commercial Li_2O_2 was also collected for comparison purposes.

2.2.5 Electrochemical Measurement

The cathodes for all tests contained 0.9-1.1 $mg\ cm^{-2}$ of Li_2O_2. Thus, the weight ratio of Li_2O_2 to carbon in the cathode was about 1:5. The cells were galvanostatically charged to 4.3 V and discharged to 2.0 V on an Arbin battery cycler with 5 minute rest time between cycles. The C-rate used for battery cycling measurements was based on the mass of Li_2O_2 present at the cathode with 1C at 1,168 $mAh\ g^{-1}$. Capacity controlled charging was done by limiting the charge duration while cycling at C/10. These cells also had charge cutoff at 4.3 V and discharge cutoff to 2 V. Cyclic voltammetry (CV) was performed on a Bio-Logic VSP potentiostat between 4.5 and 1.8 V at a scanning rate of 0.05 $mV\ s^{-1}$. Linear sweep voltammetry of the electrolyte was performed from OCV to 4.9 V in a cell with only a Celgard separator soaked with the electrolyte at a scan rate of 0.1 $mV\ s^{-1}$ with the Bio-logic potentiostat. Electrochemical impedance spectroscopy (EIS) data was collected with the Bio-Logic VSP impedance analyzer in the frequency range of 1M Hz - 0.01 Hz with Li metal foil as both counter and reference electrodes. The cells were cycled on the Arbin battery cycler at C/10 in between these tests.

2.3 Results and Discussion

The carbon sandwich type cathode configuration has been demonstrated to be effective for insulative materials like Li_2S in rechargeable Li-S batteries.[14] Active materials without binder can be sandwiched in between two layers of binder-free MWCNT or carbon paper as current collectors, which provide sufficient ion and electron transport pathways. A Li_2O_2 packed electrode can be charged to yield molecular O_2 in an open system type cell which has also been demonstrated.[15] With the known background of limited conductivity of Li_2O_2,[16] Nano24, nanosized graphitic flakes, was mixed in equal proportions by weight with Li_2O_2 to provide a conductive substrate in the sandwiched cathodes.

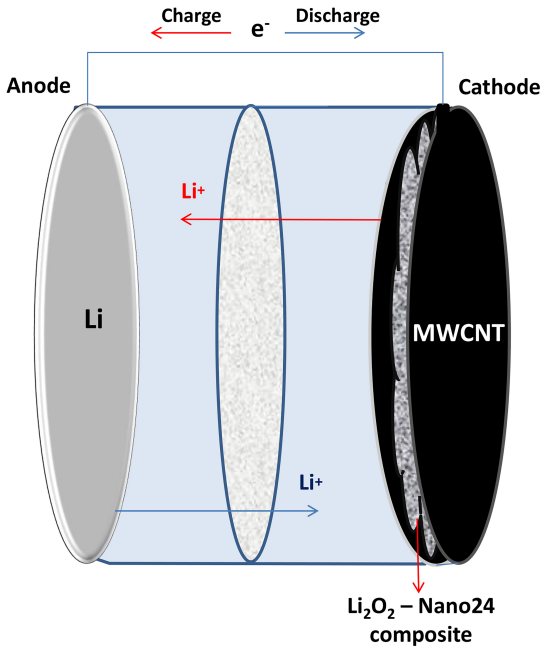

Figure 2.1. Schematic of the cell configuration. The cathode shows a buckypaper sandwich with Li_2O_2-Nano24 composite in between them.

Figure 2.1 shows the schematic of the closed system Li-O_2 battery with Li_2O_2-Nano24 composite sandwich type cathode with lithium metal foil as the anode. 1

M $LiCF_3SO_3$ in DME was selected as the electrolyte owing to low viscosity while giving high yield of Li_2O_2 during discharge.[17] This cathode configuration provides an efficient electron conduction pathway into the Li_2O_2 such that enough charge is transferred for complete conversion of Li_2O_2 to O_2. It also lowers the charge voltage below 4 V. The basis for using Nano24 was that it is a porous nanographite with high surface area (350 $m^2\ g^{-1}$) providing a large reaction surface area and thus good reaction kinetics. Also, basal surface of graphite is known to store oxygen with weak bonding.[18, 19] Carbons with higher surface area (up to 1,200 $m^2\ g^{-1}$) like Black Pearls 2000 were tested and they did not show an appreciable increase in performance.

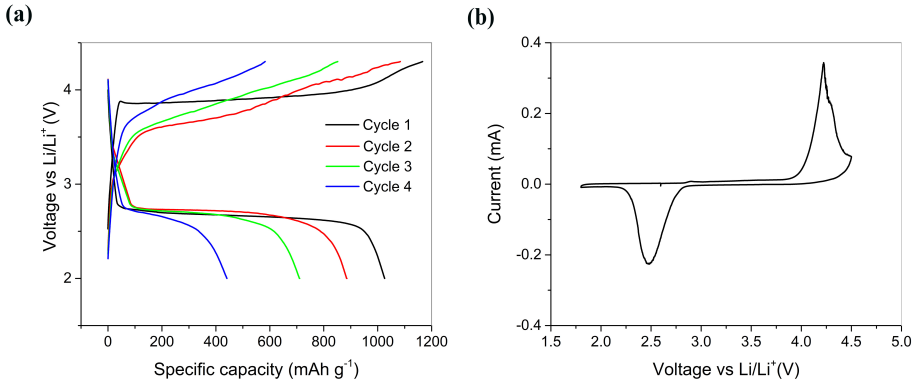

Figure 2.2. (a) Voltage profile over 4 cycles demonstrating rechargeability when cycled at C/10 rate. The rate and specific capacities are calculated based on amount of Li_2O_2 in the cathode. (b) Cyclic voltammogram of the first cycle at a sweep rate of 0.05 $mV\ s^{-1}$ showing peak voltages agreeing with charge and discharge plateaus.

Figure 2.2a shows the voltage-specific capacity profile for the first four cycles of the cell when cycled at C/10 rate. It can be seen that the first charge occurs at 3.9 V. This charge plateau is very flat and consistent till about 900 $mAh\ g^{-1}1$ after which the charge process starts terminating. At 4.3 V the process reaches the theoretical capacity for Li_2O_2 at 1,168 $mAh\ g^{-1}$. The cell shows a flat discharge voltage plateau at 2.7 V, which is consistent with other Li-O_2 cells reported in open systems.[20, 21]

The discharge process ends with fast voltage decrease to 2 V. The specific discharge capacity varies between 1,025-1,030 $mAh\ g^{-1}$. This yields a Coulombic efficiency of $\sim$ 88% for the first cycle. Thus, in the first cycle most of the Li_2O_2 charged could be formed again during discharge. It can also be calculated that 0.488 mL of oxygen gas can be evolved in the first charge considering 1 mg of Li_2O_2 at cathode and standard conditions. The DME electrolyte can dissolve a theoretical maximum of about 0.214 mL. Therefore, the produced oxygen gas could be stored by the nanographite thus causing no visible physical deformation in the cell casing due to pressure buildup. This shows that a medium that is conductive and can hold oxygen can prove to be an effective component in making a closed system battery. It is also evident that this process does involve loss of capacity, which could be due to side reactions[22, 23] and possible loss of oxygen due to imperfect containment. The contribution of side reactions will be further discussed in later sections. The second cycle charge shows a lower charging plateau at 3.7 V. This could be due to the reduction of size of the discharged Li_2O_2 particles.[24, 25] The charge terminates at a capacity of approximately 1,080 $mAh\ g^{-1}$. This capacity is slightly higher that the first discharge capacity. The extra capacity can probably be attributed to the partial rechargeablity of a decomposition product.[26] The second discharge occurs at a similar voltage as first discharge yielding a capacity of about 890 mAh g-1. This makes the Coulombic efficiency drop to about 80%. In the subsequent cycles the charge voltage increases owing to the accumulation of decomposition products on cathode. The discharge capacity reduces by 55% in 4 cycles. Though poor in terms of cycle life, this goes to demonstrate that a closed system battery is rechargeable, provided parasitic reactions are eliminated and produced oxygen during charge can be held in the cathode.

Figure 2.2b shows the first cyclic voltammogram of the cell. In the anodic sweep the current rises steeply starting at 3.9 V which corresponds to the voltage at which the first charge occurs. In the cathodic sweep, the discharge is signified by its onset at 2.7 V which also agrees with the voltage profile as seen by the galvanostatic cycling shown in Figure 2a. The cathodic peak presents the completion of the reduction

reaction of oxygen produced in the anodic sweep. The anodic peak area is similar to the cathodic peak area, indicating it is a reversible battery reaction in this closed system. To qualitatively analyze the first cycle, powder XRD was performed on an

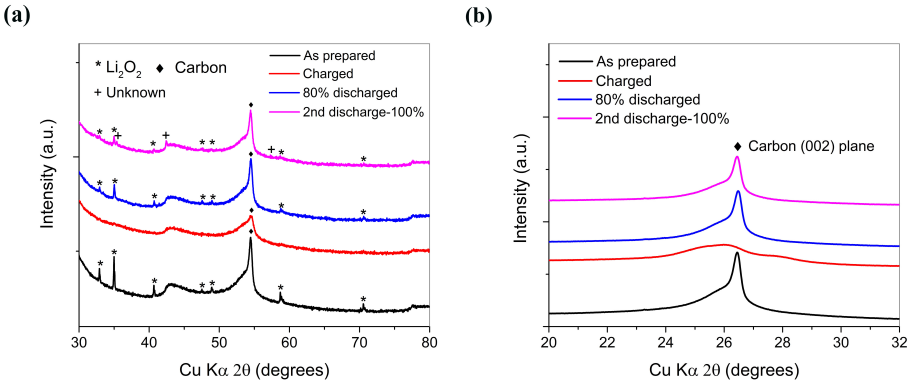

Figure 2.3. (a) Powder X-Ray Diffraction patterns of the cathode as prepared, after first charge, after first discharge by 80%, and after second discharge by 100%. (b) XRD focusing on the (002) peak of Nano24 indicative of loss of crystallinity due to O_2 adsorption in charged state. The cell was cycled at C/10 rate.

electrode as prepared without first charge, and another one after charging. XRD patterns for a cell discharged by 80% in the first cycle and a cell discharged by 100% in the second cycle were also collected. This was done so as to ascertain if the product contributing to capacity in the discharge was indeed Li_2O_2. Figure 3a shows these patterns in the 2θ range of 30° to 80° wherein the characteristic peaks of Li_2O_2 occur. The peaks before charge were matched with XRD of the commercial Li_2O_2 and ICSD pattern (Reference code: 01-074-0115). All major peaks corresponding to Li_2O_2Nano24 composite were identified and are indicated in the figure. The pattern from the charged cell shows that all the Li_2O_2 peaks have vanished leaving only the graphite (004) peak at 54.5°, indicating the complete conversion of Li_2O_2 to O_2. The discharged cells show the reappearance of all the peaks of Li_2O_2 indicating that it is regenerated in the discharge thus confirming the reversibility of this system. During the discharge to 80% in the first cycle, no impurity peaks are found. However, several

unidentified peaks are shown during the discharge to 100% in the second cycle, which means the major decomposition possibly occurs below 2.6 V in the first discharge and in the second charge. Figure 2.3b highlights the (002) plane of graphite. It is observed based on XRD peak heights that the long order crystallinity of graphite diminishes after charge but returns after discharge. This is also true with the (004) graphite plane in Figure 2.3a. This is a possible evidence of oxygen generated during the charge being physisorbed on the nanographite flakes of Nano24 through weak bonding.[27, 28] Thus in this system the nanographite works as a conductor as well as a possible oxygen storage medium. The partial matching of peaks of lithium oxalate and lithium carbonate in the XRD pattern at the end of second discharge could be due to the severe decomposition of the electrolyte in the presence of oxygen adsorbed on carbon.[18] The presence of loosely bound oxygen molecules to defect sites in the graphite of Nano24 during the charging could possibly abstract the carbon from these defect sites during discharge to form these compounds.[29] Figure 2.4 shows scanning electron microscopy images and EDS elemental (carbon and oxygen) mapping of the Li_2O_2-Nano24 composite, charged electrode sample, and discharged electrode sample. Figure 2.4a shows microsized particles of the ground Li_2O_2 particles intimately embedded in a Nano24 conductive matrix which enhances the electronic conductivity. Figure 2.4b shows the flakes of nanographite without the presence of crystalline Li_2O_2, which is consistent with the XRD result. The little content of oxygen detected in EDS mapping possibly means that some of the produced O_2 molecules could be weakly bonded to the nanographite or while most dissipated when the charged sample was exposed in the glove box and to the vacuum of the microscope. After discharge, disc- and flake-like Li_2O_2 particles are formed in the Nano24 matrix (Figure 2.4c) which is also consistent with presence of only Li_2O_2 as in the XRD result of the cell discharged by 80%. Based on the XRD, SEM, and EDS results, it is clear that Li_2O_2 as the starting material was converted to O_2 in the charge, which mostly can be held in the sandwiched electrode and reversibly converted to Li_2O_2 in the discharge. To exclude the possibility of capacity contribution by the oxidation

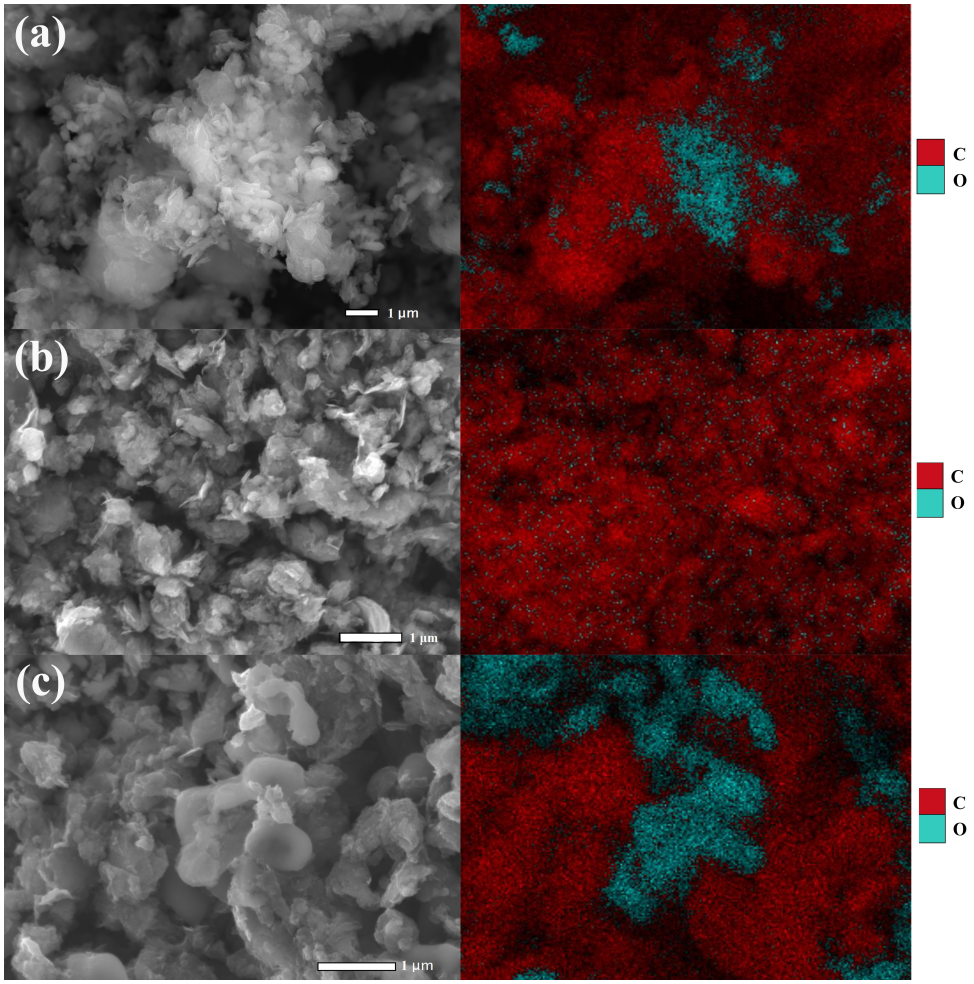

Figure 2.4. SEM images with EDS showing (a) micron sized Li_2O_2 particles with Nano24 composite (b) Nano24 flakes after charge and (c) Nanometer scale disc/flake like Li_2O_2 particles observed upon discharge. The cell was cycled at C/10 rate. SEM was performed at 80% depth of first discharge. White scale bars indicate 1μm.

of electrolyte and inactive components in the cathode, the electrolyte stability was measured by the linear voltage sweep (LVS) method and a control cell without active material in the cathode was evaluated. Figure 2.5a shows the LVS scan for 1 M $LiCF_3SO_3$ in DME. The current is less than 20 μA at 4.3 V which is the charge voltage cutoff limit for the cell with Li_2O_2. The current does not start to increase significantly until 4.8 V, indicating good stability of the electrolyte in the cell operating region.

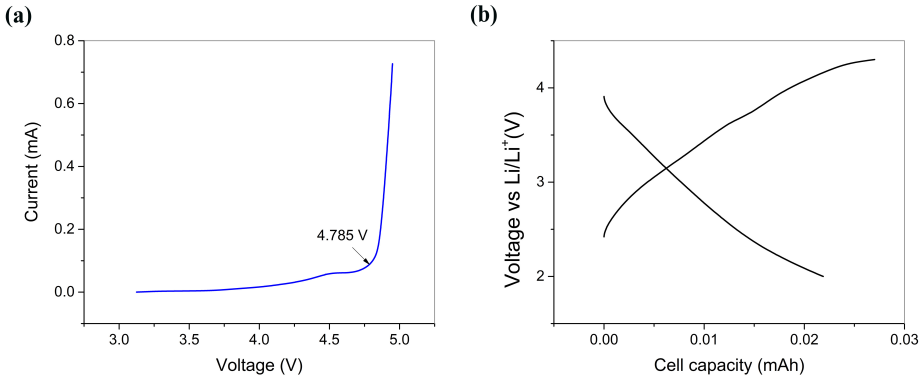

Figure 2.5. (a) Current-voltage curve of the electrolyte 1 M $LiCF_3SO_3$ in DME by the linear voltage sweep method. (b) Voltage profile for a control cell without active material to determine the capacity contribution due to other cell components.

The capacity contribution of the cell components including the two buckypaper discs was determined by cycling the control cell in the same voltage limits as the one with active material. As demonstrated in Figure 5b, neither the charge nor the discharge capacity exceeds 0.03 mAh. Thus, it can be assumed that, in the cell with Li_2O_2, the capacity contribution comes mostly from the active material Li_2O_2. To better understand the cell behavior in terms of internal resistances, electrochemical impedance spectroscopy (EIS) was performed on a cell before cycle and after first two cycles. The Nyquist plots are shown in Figure 2.6. The intercept in the high frequency range can be related to the bulk resistance of the electrolyte. The semicircles can be assigned to the charge transfer resistance.[30] The freshly-made cell shows a low bulk resistance and a low charge transfer resistance, indicating good electrical contact with Li_2O_2 in this cathode configuration. The first charge increases the charge transfer resistance significantly, which could be due to the increased resistance among three phases (solid carbon, liquid electrolyte, and gaseous adsorbed oxygen) at the cathode. The increased bulk resistance could be attributed to the resistance arising from the dissolved oxygen in the electrolyte. The extended tail at the lower frequency region is indicative of the diffusion resistance in the adsorbed oxygen in the cathode. Upon

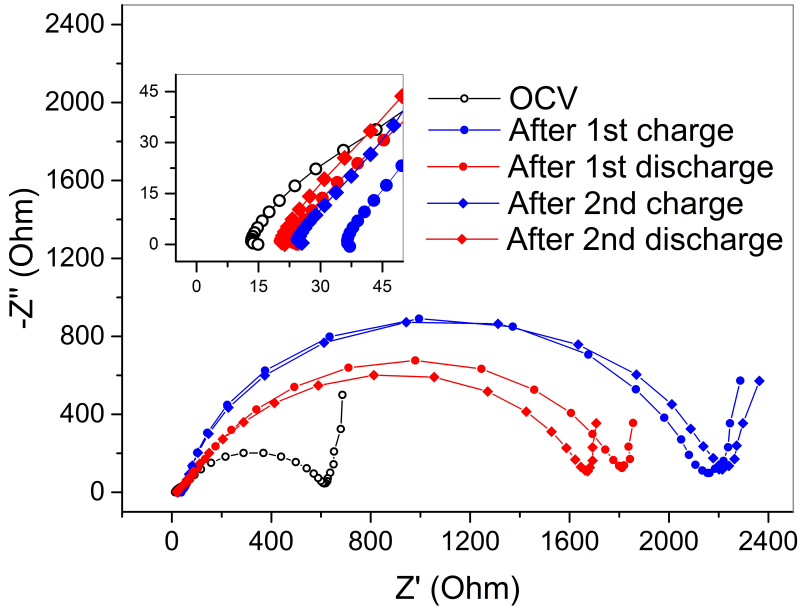

Figure 2.6. Electrochemical impedance spectroscopy analysis for a cell before and after two cycles.

discharge the bulk resistance is lowered to 20 Ω when the dissolved oxygen is converted to Li_2O_2, which can deposit on Nano24. The charge transfer resistance is still high, which can be assigned to the resistance due to the well distributed Li_2O_2 in the cathode and insulative decomposed products.[31] In the second cycle, after charge the bulk resistance is much lower than that of first charge owing to more localized absorption of O_2 due to the charging of smaller, more uniformly distributed Li_2O_2 particles during first discharge. The second discharge produces a plot similar to that of first discharge but with a slightly lower charge transfer resistance due to loss of active material. Figure 2.7 shows the first cycle data for cells cycled from C/20 to C/2 with 0.5 M $LiNO_3$ in DME electrolyte. The electrolyte (1 M $LiCF_3SO_3$ in DME) was able to support rate performance up to C/5 while the cells at higher rates failed. At C/5 1 M $LiCF_3SO_3$ in DME gave similar performance to 0.5 M $LiNO_3$ in DME. But C/2 cycling performance could only be obtained for electrolytes with $LiNO_3$

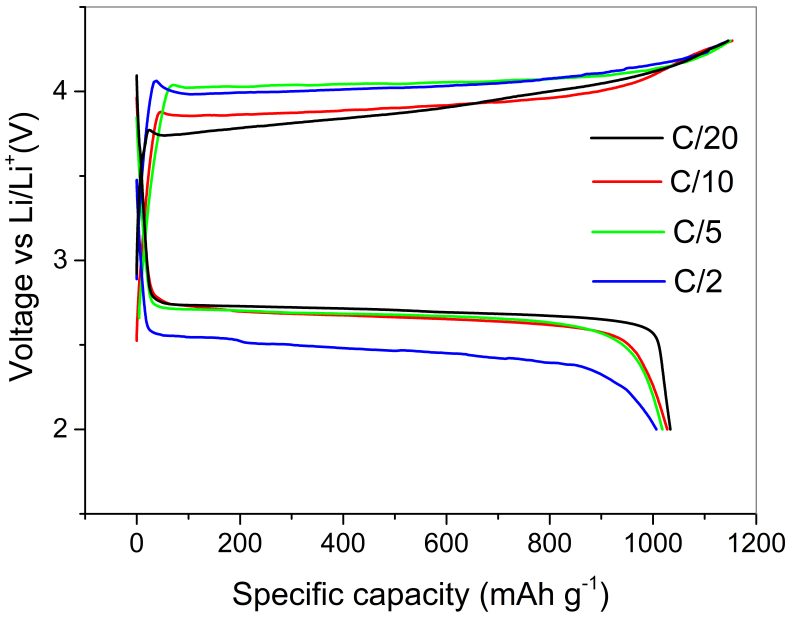

Figure 2.7. Voltage-specific capacity profiles at different C-rates with cycling based on amount of active material.

concentrations of 0.5 M or higher. All electrolytes failed to sustain cycling at 1C. This is probably due to the sluggishness of the kinetics and high cell impedances.[32] It is also interesting to note that $LiNO_3$ alone is able to sustain rate performance up to C/2. Discharge occurs at 2.7 V for C/20, C/10 and C/5 with the voltage only slightly lowering with increasing C rate. At C/2 the discharge voltage drops to about 2.5 V. The specific capacity reduction with increasing C rate is not rapid as one might expect. C/20 yields a specific capacity of 1,035 $mAh\ g^{-1}$ which reduces to 1,005 $mAh\ g^{-1}$ at C/2. This means that cell can be discharged at up to C/2 without much reduction in the specific capacity. The cell has the lowest charge overpotential of 3.8 V at C/20 which increases to 3.9 V at C/10. C/5 and C/2 seem to have similar charge plateau at 4 V. All cells charge close to the theoretical capacity of 1,168 $mAh\ g^{-1}$ indicating effective electron transport into the cathode even at higher rates. Thus,

this cathode configuration enables high Coulombic efficiency upwards of 85% even at high rates without compromising on specific energy and power.

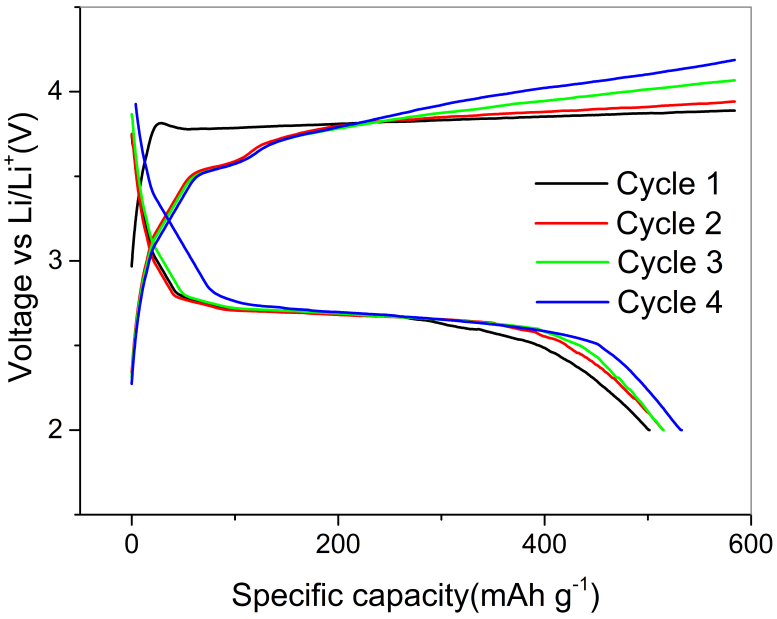

Figure 2.8. Voltage profile over 4 cycles of the closed system cell under capacity limited cycling with 50% depth of charge while cycling at C/10 rate. The specific capacities are calculated based on amount of Li_2O_2 in the cathode.

As parasitic reactions could result in severe capacity fade, an effort was made to understand cycling performance when the decomposition reactions are delayed by controlling capacity. Limiting charge by 50% would retain some unreacted Li_2O_2 on the cathode side. These remaining crystals would facilitate re-crystallization thus limiting reaction with other cell components. This strategy produces consistent cycle performance as shown in Figure 2.8. It can be seen that the cell charges to exactly 50% of theoretical capacity during charge. The first charge voltage is 3.9 V as observed in uncontrolled charging. The following discharge occurs at 2.7 V. The subsequent charges have two regions. One is a charge plateau at 3.5 V wherein the smaller particles that re-crystallized over Li_2O_2 in the first discharge are charged and

the other region of linearly increasing voltage until capacity cutoff is reached. The discharge occurs consistently at 2.7 V with capacity slowly fading, which could be due to parasitic reactions. This shows that the use of capacity limiting charge and discharge cycles, as is the protocol to delay the onset of decomposition effects, might prolong cycle life at the cost of capacity utilization.[33] As this electrode configura-

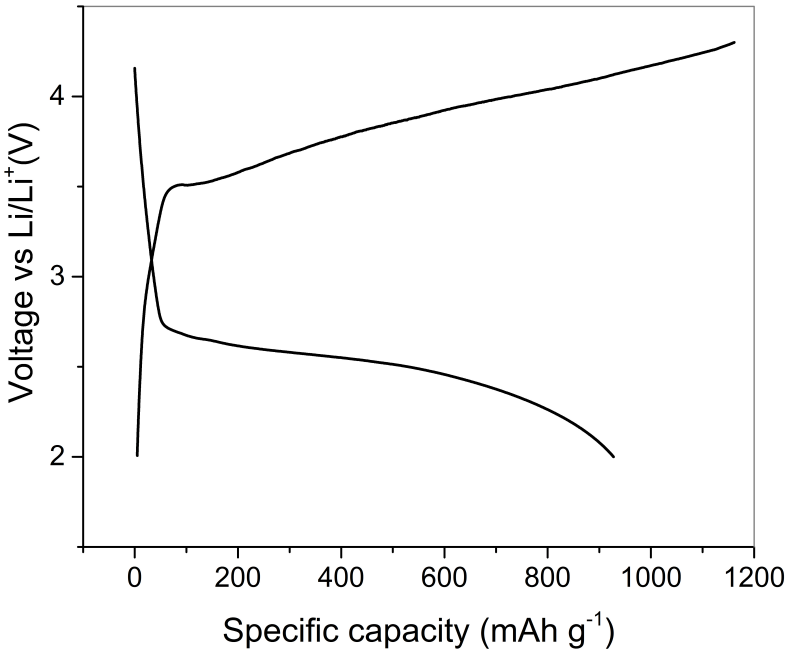

Figure 2.9. Voltage profile of full cell with Li_2O_2-Nano24 composite in sandwich cathode configuration when coupled with carbon paper anode. The specific capacities are calculated based on amount of Li_2O_2 in the cathode.

tion starts with the discharge product i.e. Li_2O_2, it permits the use of a non-Li metal anode. Present Li-ion batteries combine the cathode with graphite anode. Similarly, this cathode configuration was coupled with graphitic carbon paper as anode and EC/DEC electrolyte to obtain a full cell. The EC/DEC electrolyte was used because it is an electrolyte that can work with the graphite anode. This full cell was cycled at C/20 based on the mass of Li_2O_2 in the cathode. The first cycle performance is

shown in Figure 9. The charge starts at 3.5 V and increases linearly until it reaches the cutoff at 4.3 V at which point all the Li_2O_2 is converted to O_2 at 1,168 $mAh\ g^{-1}$. The cell discharges to 923 $mAh\ g^{-1}$. If irreversible capacity loss due to SEI layer formation34 and parasitic reactions known to occur in EC/DEC electrolyte such as Li_2O_2 decomposition[35] are taken into consideration, this cell configuration holds the promise of high Coulombic efficiency and high capacity when combined with non-Li anodes that can reversibly intercalate Li-ion in a stable electrolyte with the discharge process of Li-O_2 batteries. To gain further understanding of the charge process in

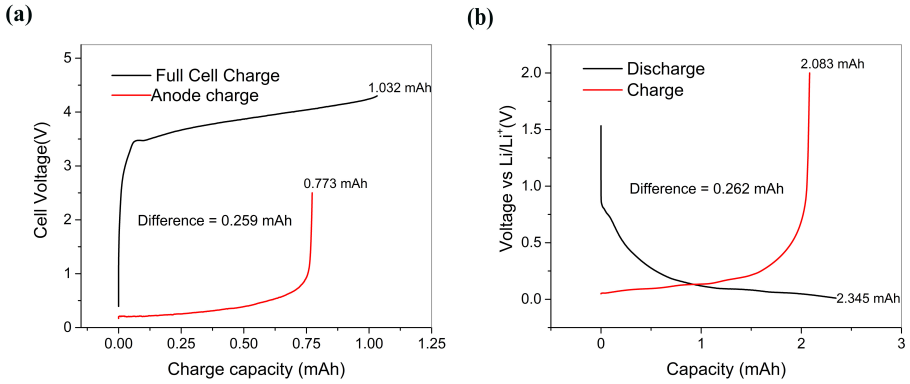

Figure 2.10. Analysis of the carbon paper anode from a full cell and a carbon paper electrode in a half cell. (a) First charge of the full cell with 0.9 mg of active material Li_2O_2 present in the cell and the recharge profile of the carbon paper anode extracted from it. (b) Voltage profile of the carbon paper electrode when tested in a half cell with lithium metal with electrolyte 1 M $LiPF_6$ in EC/DEC.

a full cell and to verify if the charge process based on equation 1.1 is indeed a two electron process the graphitic anode was further analyzed. Full cells were charged at C/20 capacity and the cells were opened on charge termination and the anode was extracted. A half-cell of this used anode was made with Li-metal foil and charged at 50 μA to a cut-off of 2.5 V to completely extract the Li intercalated during the charge process. The voltage-cell capacity profile of the first charge of a sample cell containing about 0.9 mg of Li_2O_2 and the recharge of the anode from it is shown in Figure 2.10a. It can be seen that 0.259 mAh is lost while the rest of the capacity can

be recovered. A control cell of graphitic carbon paper in a half-cell was discharged galvanostatically to 0.01 V and charged to 2 V to obtain the capacity loss at anode in SEI formation. The voltage-cell capacity profile is shown in Figure 2.10b. The first cycle of graphitic carbon paper half-cell results in a loss of 0.262 mAh. This implies that, during the first charge, all the Li can be extracted from Li_2O_2 with almost negligible side reactions. The capacity losses observed in the first discharge of half cells can be attributed to parasitic reactions which mostly occur at the end of discharge.

2.4 Conclusion

This study demonstrates that Li-O_2 batteries starting with Li_2O_2 in the binder-free sandwiched cathode configuration is rechargeable with complete conversion of its active material into its charged components. It shows that Coulombic efficiency of 85% or more is achievable if cathode is optimized. For the first time in literature, performance of a Li-O_2 cell is presented based on C-rate. A high discharge capacity of over 1,000 $mAh\ g^{-1}$ can be obtained in the first discharge. A strategy to extend cycle life while sacrificing cell capacity is demonstrated. The capability of using this configuration with graphite anode in a full cell with efficient charge process is also shown. The analysis of the charged graphite anode indicates that there is negligible capacity contribution due to the side reactions in the first charge of Li_2O_2.[34]

The study fundamentally presents a new paradigm to better understand Li-O_2 batteries. This approach can be utilized to understand the reaction kinetics, electrolyte-cathode interaction, and parasitic reactions. It can also be used to study the use of oxygen storage materials, different electrolytes and non-Li anodes in such batteries. This approach eliminates the need for oxygen extraction/storage and purification equipment used in current Li-O_2 cell design. Closed system Li-O_2 batteries, although possessing lower specific energy than its open system counterpart, could be a step towards practical implementation of this technology.

2.5 References

[1] J. B. Goodenough and K.-S. Park, "The Li-ion rechargeable battery: a perspective," *Journal of the American Chemical Society,* vol. 135, pp. 1167-1176, 2013.

[2] A. Manthiram, "Materials Challenges and Opportunities of Lithium Ion Batteries," *The Journal of Physical Chemistry Letters,* vol. 2, pp. 176-184, 2011.

[3] P. G. Bruce, S. A. Freunberger, L. J. Hardwick, and J.-M. Tarascon, "Li-O2 and Li-S batteries with high energy storage," *Nature Materials,* vol. 11, pp. 19-29, 2012.

[4] D. G. Kwabi, N. Ortiz-Vitoriano, S. A. Freunberger, Y. Chen, N. Imanishi, P. G. Bruce*, et al.*, "Materials challenges in rechargeable lithium-air batteries," *MRS Bulletin,* vol. 39, pp. 443-452, 2014.

[5] S. D. Beattie, D. M. Manolescu, and S. L. Blair, "High-Capacity Lithium–Air Cathodes," *Journal of The Electrochemical Society,* vol. 156, pp. A44-A47, 2009.

[6] R. S. Assary, K. C. Lau, K. Amine, Y.-K. Sun, and L. A. Curtiss, "Interactions of Dimethoxy Ethane with Li2O2 Clusters and Likely Decomposition Mechanisms for Li–O2 Batteries," *The Journal of Physical Chemistry C,* vol. 117, pp. 8041-8049, 2013.

[7] G. Bieker, P. M. Bieker, and M. Winter, "Electrochemical In Situ Investigations of the SEI and Dendrite Formation on the Lithium Metal Anode," *Physical Chemistry Chemical Physics,* vol. 17, pp. 8670-9, 2015.

[8] A. C. Luntz and B. D. McCloskey, "Nonaqueous Li–Air Batteries: A Status Report," *Chemical Reviews,* vol. 114, pp. 11721-11750, 2014.

[9] G. Girishkumar, B. McCloskey, A. C. Luntz, S. Swanson, and W. Wilcke, "Lithium−Air Battery: Promise and Challenges," *The Journal of Physical Chemistry Letters,* vol. 1, pp. 2193-2203, 2010.

[10] D. G. Kwabi, T. P. Batcho, C. V. Amanchukwu, N. Ortiz-Vitoriano, P. Hammond, C. V. Thompson*, et al.*, "Chemical Instability of Dimethyl Sulfoxide in Lithium–Air Batteries," *The Journal of Physical Chemistry Letters,* vol. 5, pp. 2850-2856, 2014.

[11] Y. Fu and A. Manthiram, "Silicon nanoparticles supported on graphitic carbon paper as a hybrid anode for Li-ion batteries," *Nano Energy,* vol. 2, pp. 1107-1112, 2013.

[12] Y. Fu, Y.-S. Su, and A. Manthiram, "Li2S-Carbon Sandwiched Electrodes with Superior Performance for Lithium-Sulfur Batteries," *Advanced Energy Materials,* vol. 4, p. 1300655, 2014.

[13] T. Ogasawara, A. Débart, M. Holzapfel, P. Novák, and P. G. Bruce, "Rechargeable Li2O2 Electrode for Lithium Batteries," *Journal of the American Chemical Society,* vol. 128, pp. 1390-1393, 2006.

[14] M. D. Radin, J. F. Rodriguez, F. Tian, and D. J. Siegel, "Lithium Peroxide Surfaces Are Metallic, While Lithium Oxide Surfaces Are Not," *Journal of the American Chemical Society,* vol. 134, pp. 1093-1103, 2012.

[15] B. McCloskey, D. Bethune, R. Shelby, G. Girishkumar, and A. Luntz, "Solvents' critical role in nonaqueous lithium–oxygen battery electrochemistry," *The Journal of Physical Chemistry Letters,* vol. 2, pp. 1161-1166, 2011.

[16] Y.-J. Xu and J.-Q. Li, "The interaction of molecular oxygen with active sites of graphite: a theoretical study," *Chemical Physics Letters,* vol. 400, pp. 406-412, 2004.

[17] P. Heiney, P. Stephens, S. Mochrie, J. Akimitsu, R. Birgeneau, and P. Horn, "X-ray study of molecular oxygen adsorbed on graphite," *Surface Science,* vol. 125, pp. 539-564, 1983.

[18] K. Abraham and Z. Jiang, "A polymer electrolyte-based rechargeable lithium/oxygen battery," *Journal of The Electrochemical Society,* vol. 143, pp. 1-5, 1996.

[19] H.-G. Jung, J. Hassoun, J.-B. Park, Y.-K. Sun, and B. Scrosati, "An improved high-performance lithium–air battery," *Nature Chemistry,* vol. 4, pp. 579-585, 2012.

[20] S. A. Freunberger, Y. Chen, N. E. Drewett, L. J. Hardwick, F. Bardé, and P. G. Bruce, "The Lithium–Oxygen Battery with Ether-Based Electrolytes," *Angewandte Chemie International Edition,* vol. 50, pp. 8609-8613, 2011.

[21] B. McCloskey, D. Bethune, R. Shelby, T. Mori, R. Scheffler, A. Speidel*, et al.*, "Limitations in rechargeability of Li-O2 batteries and possible origins," *The Journal of Physical Chemistry Letters,* vol. 3, pp. 3043-3047, 2012.

[22] B. M. Gallant, D. G. Kwabi, R. R. Mitchell, J. Zhou, C. V. Thompson, and Y. Shao-Horn, "Influence of Li2O2 morphology on oxygen reduction and evolution kinetics in Li-O2 batteries," *Energy & Environmental Science,* vol. 6, pp. 2518-2528, 2013.

[23] Y. Hu, X. Han, F. Cheng, Q. Zhao, Z. Hu, and J. Chen, "Size effect of lithium peroxide on charging performance of Li-O2 batteries," *Nanoscale,* vol. 6, pp. 177-180, 2014.

[24] S. Xu, S. K. Das, and L. A. Archer, "The Li-CO2 battery: a novel method for CO2 capture and utilization," *RSC Advances,* vol. 3, pp. 6656-6660, 2013.

[25] D. C. Sorescu, K. D. Jordan, and P. Avouris, "Theoretical Study of Oxygen Adsorption on Graphite and the (8,0) Single-walled Carbon Nanotube," *The Journal of Physical Chemistry B,* vol. 105, pp. 11227-11232, 2001.

[26] C. Hontoria-Lucas, A. J. López-Peinado, J. d. D. López-González, M. L. Rojas-Cervantes, and R. M. Martín-Aranda, "Study of oxygen-containing groups in a series of graphite oxides: Physical and chemical characterization," *Carbon,* vol. 33, pp. 1585-1592, 1995.

[27] S. M. Lee, Y. H. Lee, Y. G. Hwang, J. Hahn, and H. Kang, "Defect-induced oxidation of graphite," *Physical Review Letters,* vol. 82, p. 217, 1999.

[28] G. Zhang, J. Zheng, R. Liang, C. Zhang, B. Wang, M. Hendrickson*, et al.*, "Lithium–air batteries using SWNT/CNF buckypapers as air electrodes," *Journal of the Electrochemical Society,* vol. 157, pp. A953-A956, 2010.

[29] B. D. McCloskey, A. Speidel, R. Scheffler, D. C. Miller, V. Viswanathan, J. S. Hummelshøj*, et al.*, "Twin Problems of Interfacial Carbonate Formation in Nonaqueous Li–O2 Batteries," *The Journal of Physical Chemistry Letters,* vol. 3, pp. 997-1001, 2012.

[30] V. Viswanathan, J. K. Nørskov, A. Speidel, R. Scheffler, S. Gowda, and A. C. Luntz, "Li–O2 Kinetic Overpotentials: Tafel Plots from Experiment and First-Principles Theory," *The Journal of Physical Chemistry Letters,* vol. 4, pp. 556-560, 2013.

[31] H.-D. Lim, K.-Y. Park, H. Gwon, J. Hong, H. Kim, and K. Kang, "The potential for long-term operation of a lithium-oxygen battery using a non-carbonate-based electrolyte," *Chemical Communications,* vol. 48, pp. 8374-8376, 2012.

[32] R. Fong, U. von Sacken, and J. R. Dahn, "Studies of Lithium Intercalation into Carbons Using Nonaqueous Electrochemical Cells," *Journal of The Electrochemical Society,* vol. 137, pp. 2009-2013, 1990.

[33] S. A. Freunberger, Y. Chen, Z. Peng, J. M. Griffin, L. J. Hardwick, F. Bardé*, et al.*, "Reactions in the Rechargeable Lithium–O2 Battery with Alkyl Carbonate Electrolytes," *Journal of the American Chemical Society,* vol. 133, pp. 8040-8047, 2011.

[34] A. Bhargav and Y. Fu, "Lithium Peroxide-Carbon Composite Cathode for Closed System Li-O2 Batteries," *Journal of The Electrochemical Society,* vol. 162, pp. A1327-A1333, 2015.

3. CHEMICALLY SYNTHESIZED LITHIUM PEROXIDE-CNF COMPOSITE CATHODE

3.1 Introduction

Lithium-ion batteries have transformed our world by ushering in the age of portable electronics and has made all electric and hybrid vehicles a viable technology. Lithium-oxygen (Li-O_2) chemistry is an attractive high energy density battery technology that can possibly meet our needs.[1] Despite this, current Li-O_2 batteries face many challenges such as severe electrolyte and cathode decomposition at high overpotentials,[2] electrolyte loss due to constant purging of oxygen (O_2) gas,[3] and loss of active sites in the cathode due to build-up of insulating discharge products.[4, 5] Also, a practical implementation of Li-O_2 batteries would require associated systems to extract, purify, store and deliver pure O_2 gas with minimal water (H_2O) and carbon dioxide (CO_2) from intake air.[6] The high amount of electrolyte used to compensate for the electrolyte loss and the paraphernalia associated with O_2 delivery significantly reduces the specific energy of the cell and increases the cost of the system. The other aforementioned challenges result in low energy efficiency and reduced cycle life.[7] Although high energy densities are quoted for Li-O_2 systems based on the active material i.e. O_2 being derived from the air instead of being stored within the cell, it is only practical to assume energy densities based on practical loading/formation of the end product lithium peroxide (Li_2O_2) in the cathode at the end of discharge as this determines the final weight of the battery.[8] A recent viewpoint appropriately highlights the incongruity in literature on the reporting of Li-O_2 performance.[9] Closed system Li-O_2 cells using Li_2O_2 (theoretical capacity: 1,168 $mAh\ g^{-1}$) as a starting material in the cathode without external supply of oxygen can avoid normalization of capacity based on inactive materials, utilize deep discharge even under capacity

controlled regime, and ascertain discharge capacity is only due to active materials. Thus, closed system Li-O2 batteries provide more practical performance metrics that can be expected from this battery technology.

Li_2O_2 containing cathodes have been studied earlier to confirm O_2 evolution on charging,[10] understand catalysis,[11-13] cathode interfaces,[14] properties of discharge products,[15] and stability of binders.[16] However, prolonged cycle life was not demonstrated in these works. Our earlier work introduced the concept of a closed system Li-O_2 battery wherein using Li_2O_2 as the starting active material would minimize the above stated problems.[17] Such a system enables the use of Li_2O_2 to generate oxygen within the cell. It also minimizes the amount of electrolyte used and thus increases the practical specific energy achievable by the Li-O_2 system. In this work, we have chemically synthesized nanocrystalline Li_2O_2 particles that are embedded in self-weaving carbon nanofibers (CNFs) to form a free standing, binder free, and current collector free composite cathode. This cathode exhibits a significantly improved cell performance from the earlier report due to lower carbon to Li_2O_2 ratio, optimized electrolyte, smaller particle size and better distribution of Li_2O_2. The carbon nanofiber provides excellent electrical conduction and mechanical strength to accommodate volume changes during battery operation. This cathode eliminates binders which have been proven to be detrimental in Li-O_2 battery operation.[18]

3.2 Experimental

3.2.1 Materials

Graphitized carbon nanofiber (CNF) (D L 100 nm 20-200 μm, Sigma-Aldrich), lithium hydroxide monohydrate (LiOH·H_2O, 98+%, Acros Organics), hydrogen peroxide solution (H_2O_2, 50 wt. % in H_2O, Sigma-Aldrich), methanol (CH_3OH, low water, Fisher Chemical), lithium trifluoromethanesulfonate ($LiCF_3SO_3$, 98%, Acros Organics), lithium nitrate ($LiNO_3$, 99+%, Acros Organics), and 1,2-dimethoxyethane (DME, anhydrous, 99.5%, Sigma-Aldrich) were purchased and used as received.

3.2.2 Cathode Preparation

Lithium hydroxide monohydrate was dissolved in 100 mL methanol to prepare 0.1 M LiOH solution. 100 mg of CNF was first vigorously stirred into the lithium hydroxide solution to disperse it. This mixture was then ultrasonicated using a vibracell VC505 sonicator for 15 minutes causing the CNF to interweave. 15 mol % excess (with respect to LiOHH_2O) of 50% hydrogen peroxide solution was added dropwise into the dispersion under vigorous stirring at 35°C to form the composite consisting of $Li_2O_2 \cdot H_2O_2 \cdot 3H_2O \cdot 8CH_3OH$ in CNF. The products were vacuum filtered on to a 7 cm filter paper and washed repeatedly with methanol and ethanol. The cathodes thus formed were free-standing, flexible films of approximately 350 micron thickness and 7 cm in diameter. The cathode was dried under vacuum at $100 - 110$°C for 24 h to obtain the Li_2O_2-CNF composite cathode that was quickly transferred into the glovebox with minimal exposure to air for further handling and testing.

3.2.3 Materials Characterization

The Li_2O_2 content in the cathode was determined by thermogravimetric analysis (TGA) performed on a TA instruments SDT Q600 analyzer under argon gas flow at 50 mL min^{-1} while heating from 25°C to 600°C at 110°C min^{-1}. For comparison, TGA was also performed on mechanically ground Li_2O_2 powder and CNF mixed in appropriate ratios. TGA samples were transferred in alumina crucibles in sealed, argon filled vials. X-Ray Diffraction (XRD) was performed on a Bruker D8 Discover diffractometer with Cu Kα radiation source for 2θ between 20° and 80° at a scan rate of $1.25°min^{-1}$. The XRD samples were prepared in the glovebox by washing the cathode several times with pure DME, dried in the glovebox and covered with a Kapton film to prevent any exposure to air. Scanning electron microscopy (SEM) was performed with a JEOL JSM-7800F field emission scanning electron microscope equipped with energy-dispersive X-ray spectroscopy (EDS). SEM samples were mounted inside the glovebox after washing and drying and the samples were transferred to the microscope

in an argon filled sealed container. The cells used for *ex-situ* characterizations were appropriately cycled at C/10 rate before opening them to extract the cathode.

3.2.4 Cell Assembly

The Li_2O_2-CNF samples were cut into 7/16 inch cathode disks without additional current collectors. Electrodes were weighed before cell assembly to determine the mass of Li_2O_2 present. The electrodes weighed between 3 mg to 4.5 mg. The weight percent of Li_2O_2 in the sample obtained from TGA analysis was used to determine the active material loading in the cathode. An electrolyte consisting of 0.5 M $LiCF_3SO_3$ and 0.5 M $LiNO_3$ in DME was prepared. CR2032 coin cells were assembled with the binder-free, current collector-free, free standing flexible composite film as the cathode. 50 μL of the electrolyte was added to this cathode and a Celgard 2400 separator was placed on it. An additional 30 μL of electrolyte was added before placing the Li-foil anode with a nickel foam current collector to complete the cell for crimping. The handling of the cathode and cell assembly were performed in an M-Braun glovebox with oxygen and water content less than 0.1 ppm.

3.2.5 Electrochemical Measurement

The coin cells were galvanostatically cycled on an Arbin battery cycler at the appropriate C-rate calculated based on the active material loading on the cathode. The cells were galvanostatically charged to 4.3 V and discharged to 2.0 V on an Arbin battery cycler with 5 minute rest time between cycles. The C-rate used for battery cycling measurements was based on the mass of Li_2O_2 present at the cathode with 1C at 1,168 $mA\ g^{-1}$. Capacity controlled charging was done by limiting the charge duration while cycling at C/10. These cells also had charge cutoff at 4.3 V and discharge cutoff to 2 V. Cyclic voltammetry (CV) was performed on a Bio-Logic VSP potentiostat between 4.3 and 2.0 V at a scanning rate of 0.05 $mV\ s^{-1}$. Electrochemical impedance spectroscopy (EIS) data was collected with the Bio-Logic

VSP impedance analyzer in the frequency range of 1M Hz - 0.01 Hz with Li metal foil as both counter and reference electrodes. The cells were cycled on the Arbin battery cycler at C/10 in between these tests.

3.3 Results and Discussion

Lithium peroxide can be synthesized by the addition of hydrogen peroxide (H_2O_2) to lithium hydroxide monohydrate ($LiOH{\cdot}H_2O$) in the presence of an alcohol medium such as methanol (CH_3OH) to form lithium hydroperoxide ($Li_2O_2 \cdot H_2O_2 \cdot 3H_2O \cdot 8CH_3OH$) which, on drying *in-vaccuo*, yields high purity Li_2O_2.[19] Thus by combining the synthesis of Li_2O_2 and facile dispersion of CNF in methanol we have developed a versatile and green cathode preparation technique that is easily scalable for preparing high performance Li_2O_2 composite cathodes. Figure 3.1 shows the schematic

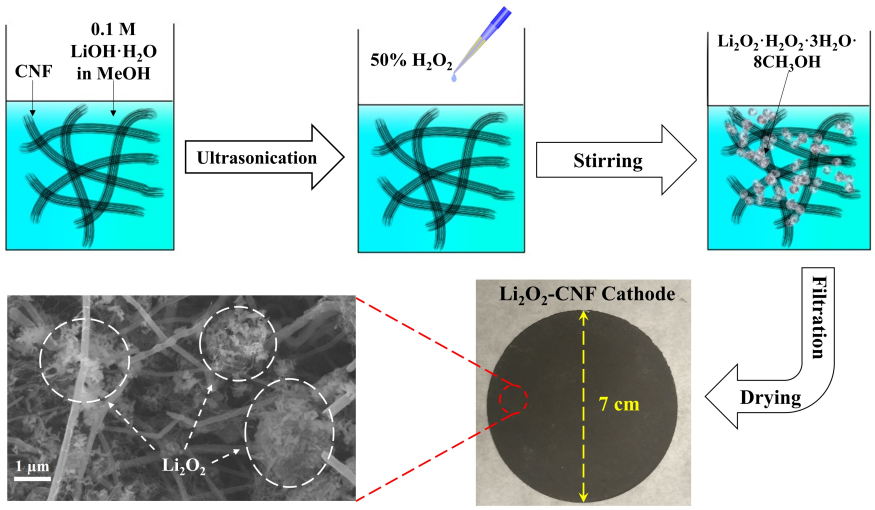

Figure 3.1. Schematic outlining the Li_2O_2-CNF composite cathode synthesis, photograph showing the large binder-free composite cathode, and SEM image showing nanocrystalline Li_2O_2 particles embedded in the CNF network.

representation of this process. The process of cathode fabrication consisted of dispersing the CNF bundles in a methanolic solution of lithium hydroxide. The methanol

alleviates the hydrophobic behaviour of CNFs and facilitates easy dispersion. This was followed by ultrasonication which assists the weaving of the CNFs. The addition of excess of 50% of H_2O_2 ensures the complete conversion of all lithium hydroxide to lithium hydroperoxide. The interwoven CNFs are effective in trapping and confining the lithium hydroperoxide particles as they precipitate out of the solution. On filtration and drying the Li_2O_2-CNF composite cathode was obtained. It consists of agglomerates of nanocrystalline Li_2O_2 particles. Thermogravimetric analysis of the cathode (Figure 3.2) revealed that 35 wt.% of the cathode consisted of Li_2O_2.[16] CR2032 coin cells were assembled with this cathode (see ESI for cell assembly pro-

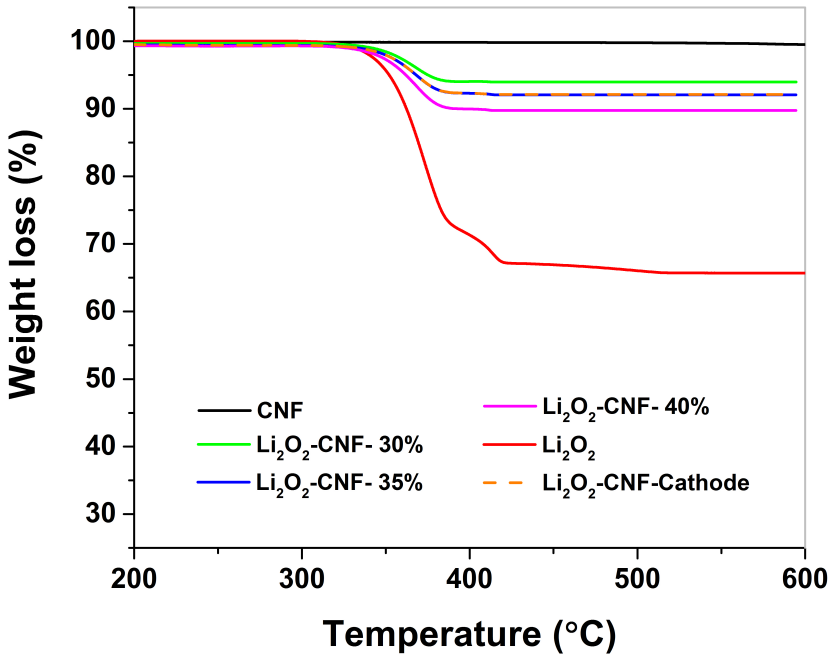

Figure 3.2. Thermogravimetric analysis of CNT, premixed LiLi_2O_2-CNF composites, pure Li_2O_2, and the Li_2O_2-CNF cathode sample.

cedure) and 0.5 M lithium trifluoromethane sulfonate (lithium triflate, $LiCF_3SO_3$) and 0.5 M lithium nitrate ($LiNO_3$) in dimethoxyethane (DME) as the electrolyte. This composition of the electrolyte was chosen because higher donor numbers (DN)

of triflate and nitrate anions would increase cell capacity through intermediate species solvation.[20] The voltage profile for the cell cycled at C/10 (Figure 3.3a) shows a

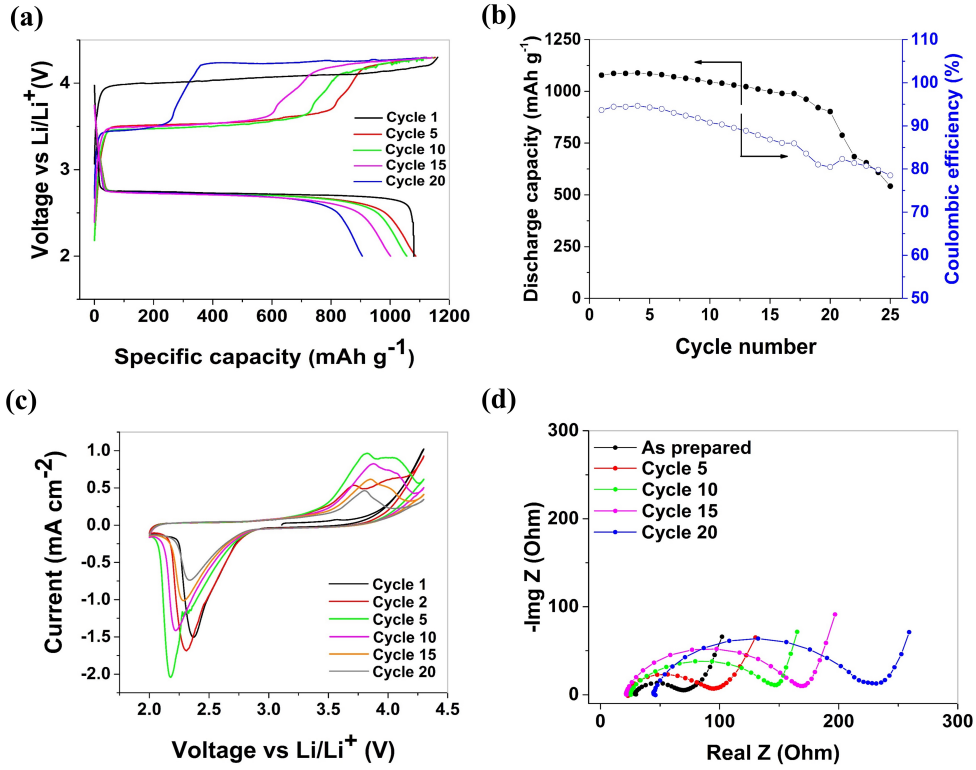

Figure 3.3. (a) Voltage profile of the cell cycled at C/10 (1C = 1168 $mA\ g^{-1}$ based on Li_2O_2 mass), (b) cycle performance of the same cell, (c) cyclic voltammogram of the cathode performed at 0.1 $mV\ s^{-1}$, and (d) EIS spectra of discharged cells cycled at C/10.

4 V plateau for the first charge. This high overpotential is due to agglomeration of the synthesized Li_2O_2 particles. The charge terminates at 4.3 V at a specific charge capacity of 1,158 $mAh\ g^{-1}$ (based on Li_2O_2 mass in the cathode) demonstrating almost complete conversion of Li_2O_2 to O_2. This capacity is lower than the theoretical capacity of 1,168 $mAh\ g^{-1}$ probably due to errors in Li_2O_2 mass measured based on TGA results and the presence of impurities. The oxygen evolved in charge was stored in the graphitic CNF thus producing no visible deformation in the cell casing. The discharge occurs at 2.7 V with a sudden voltage drop occurring on deep discharge to 2

V at 1,080 $mAh\ g^{-1}$. This cathode exhibits a high Coulombic efficiency of 93% for the first cycle. This implies loss of capacity due to electrolyte decomposition and cathode degradation at high overpotentials.[21] Subsequent cycles clearly show two voltage plateaus during charge. The first one occurring at about 3.5 V which is attributable to the conversion of the uniformly distributed Li_2O_2 to O_2 and the next occurring at 4.2 V probably due to conversion of Li_2CO_3 to CO_2.[22, 23] As the cycling progresses the 3.5 V plateau diminishes and 4.2 V plateau becomes prominent implying electrode passivation due to electrolyte decomposition products which degrades cell performance until cell death. The 2.7 V reduction plateau is not altered due to the closeness of the reduction potential of CO_2 with that of O_2.[23] Figure 3.3b shows the cycling performance of the cell and reflects the effects seen in the voltage profile. The cell maintains a high discharge capacity of >1000 $mAh\ g^{-1}$ and Coulombic efficiency of >85% over 18 cycles, then the capacity diminishes as the cell is cycled with lowering of efficiency until the 20th cycle. Beyond this, the cell capacity deteriorates rapidly owing to severe cathode passivation. The cell still exhibits efficiencies near 80% due to the proportional decrease in charge capacity. The cell completely failed beyond the 28th cycle exhibiting no rechargeability (not shown). The cyclic voltammogram of the cathode (Figure 3.3c) corroborates the voltage profile. The 1st oxidation occurs at 4 V and the first reduction occurs at 2.7 V. By the 2nd oxidation, a distinct 3.5 V peak is visible with a minor peak at 4.2 V. In the 5th cycle, the predominant peak is at 3.5 - 3.7 V region corresponding to the oxidation of Li_2O_2. The reduction peak shows a shift to lower voltage due to the electrode passivation causing increased ohmic polarization. As cycling progresses, the 3.5 V peak height diminishes and the oxidation occurs at 4.2 V showing that Li_2CO_3 decomposition is the predominant process.[24] To further understand the effect of electrode passivation, electrochemical impedance spectroscopy (EIS) of the cathode discharged to different cycles was performed. The results in Figure 2d shows low charge transfer resistance (diameter of the semicircle) in the fresh, uncycled cell. Thus, the CNFs provide abundant electron pathways into the Li_2O_2 particles. As the cell was cycled, the semicircle diameter

increases thus supporting the increased charge overpotential observed in the voltage profile. After 20 cycles, there is nearly a 4 fold increase of charge transfer resistance along with increased electrolyte resistance meaning severe electrolyte decomposition and cathode passivation to the extent of reduced Li-ion conductivity supported by the electrolyte.

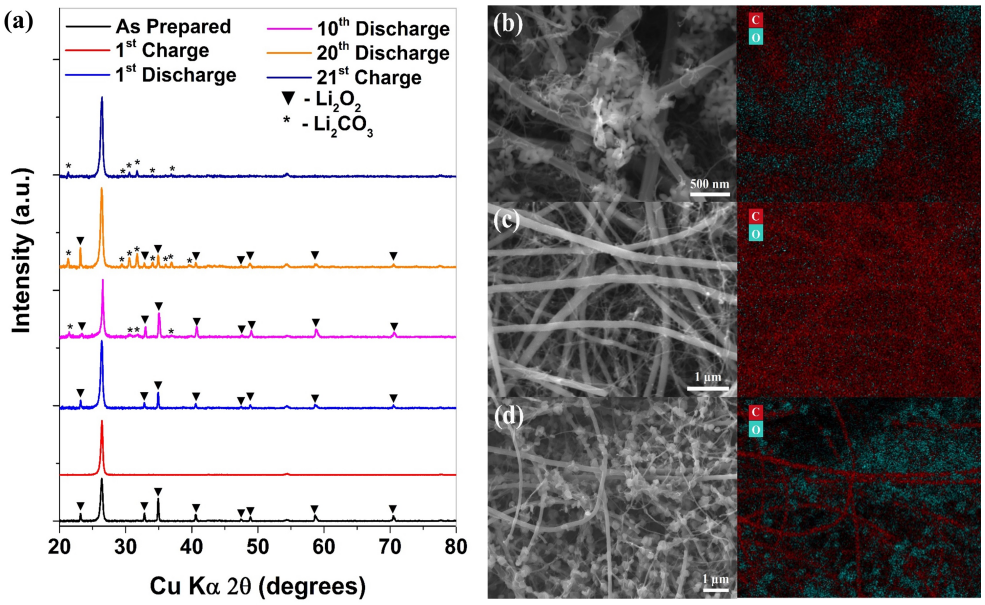

Figure 3.4. (a) XRD patterns for the as-synthesized cathode and the cathode discharged/charged to different cycles at C/10, SEM images and EDX mapping of the (b) as-synthesized cathode, (c) completely charged cathode, and (d) completely discharged cathode. Blue represents oxygen and red represents carbon in the EDX map.

X-ray diffraction (XRD) was performed to prove the above hypothesis of formation of both Li_2O_2 and Li_2CO_3 and to explain the sustained cycling even in the presence of Li_2CO_3, as shown in Figure 3.4a.The XRD of the as-synthesized cathode clearly exhibits all the peaks of Li_2O_2 without any impurity peaks. On charging the cathode, no Li_2O_2 peaks are detected confirming the conversion of all Li_2O_2 to O_2. On discharging all Li_2O_2 peaks return and no impurities can be detected. But on further cycling, at the 10th discharge, when significant portion of the voltage profile

covers the 4.2 V plateau, traces of Li_2CO_3 can be seen in the discharged cathode. At the 20th discharge, when Li_2CO_3 formation predominates, clear signals for all major peaks for Li_2CO_3 are observed while other possible by-products were not detected. We believe that the high DN of anions in the electrolyte promotes CO_2 dissolution and solvation of intermediates hypothesized in literature leading to Li_2CO_3 formation.[25, 26] Also, discharged products could consist of reversible and conductive Li_2O_2@Li_2CO_3 interfaces formed on the cathode due to reaction between O_2 and CNF in the presence of Li-ions during discharge.[27] On charging this cathode, Li_2O_2 peaks disappear and Li_2CO_3 peaks show clear reduction in intensity. Some peaks of Li_2CO_3 are not present anymore. We hypothesize that this observation could be due to a part of Li_2CO_3 in the form of Li_2O_2@Li_2CO_3 interfaces being converted to CO_2 upon charging. The residual Li_2CO_3 peaks arise from its deposition on the carbon cathode due to further irreversible electrolyte decomposition. From the XRD analysis, it appears that the cell could operate through reversible formation and decomposition of both Li_2O_2 and Li_2CO_3.[23, 26]

To better understand the morphological changes in the Li_2O_2-CNF cathode during cycling, scanning electron microscopy (SEM) was performed and EDX mapping of the cathode was done to identify Li_2O_2 particles. The as-synthesized cathode in Figure 3.4b shows the agglomerates of nanocrystalline Li_2O_2 forming micrometer-sized particles which are well embedded in the CNF network. The electrical conductivity in this cathode architecture is enhanced by both the CNFs and small size of Li_2O_2.[28] No presence of Li_2O_2 is detected on charging the cathode (Figure 3.4c) indicating the conversion of all Li_2O_2 to O_2. On the 1st discharge (Figure 3.4d), Li_2O_2 particles formed from O_2 reduction are evenly distributed throughout the cathode. These particles vary from 100 to 200 nm and appear like platelets (Figure 3.5). The presence of high donor number anions and minimal moisture have led to the formation of Li_2O_2 platelets through the solution mediated mechanism reported in literature.[29] The near uniform size and distribution of Li_2O_2 particles after the 1st discharge help lower the oxidation potential to 3.5 V in the 2nd charge as shown in Figure 3.3a.

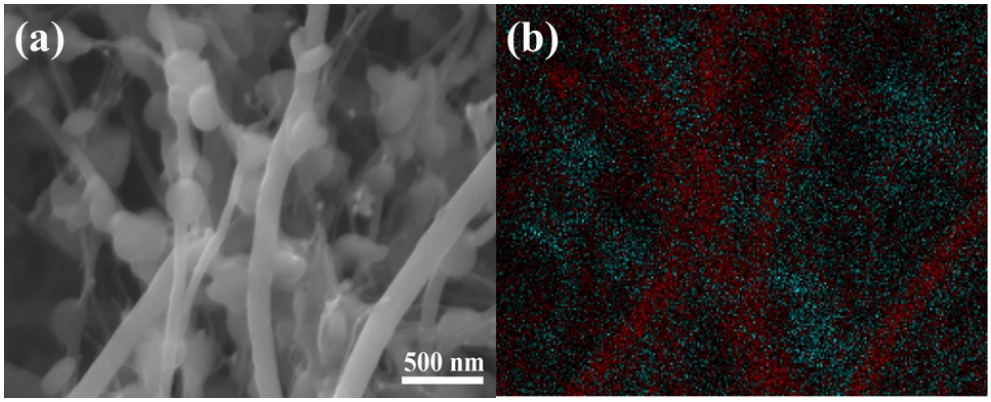

Figure 3.5. High magnification SEM showing (a) the Li_2O_2 platelets formed during discharge with (b) EDX mapping of the same. Blue represents oxygen and red represents carbon in the EDX map.

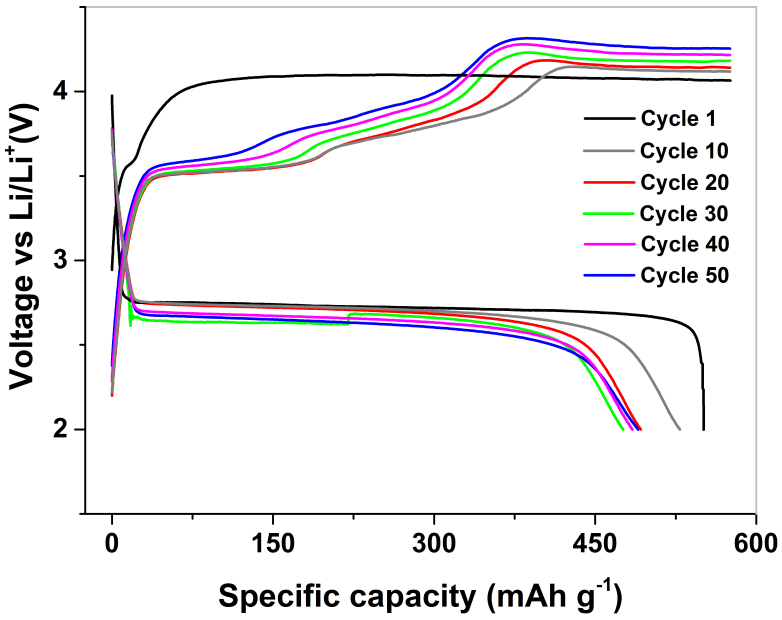

Figure 3.6. Voltage profile of charge capacity limited cell cycled at C/10 showing increased charge voltage and reduced discharge voltage as cell is cycled to 50 cycles. Charge capacity was limited to 50% of theoretical charge capacity of the cathode (1 C = 1,168 $mA\ g^{-1}$).

Based on the voltage profile in Figure 3.3a and XRD results from Figure 3.4a, it is clear that the electrolyte decomposition is aggravated only when the battery operates at high charge overpotentials. The electrolyte decomposition and cathode degradation can be minimized if the cell is operated at lower voltages. [22] One way to do this is to use capacity limited charging protocol. Cells were cycled at a given rate such that only 50% of the theoretical capacity of the cathode was utilized. The charge voltage cut-off was set to 4.3 V to enable the activation of the Li_2O_2 and accumulated Li_2CO_3. This protocol would thus enable the usage of the lower charge plateau for majority of the charge process minimizing parasitic reactions(Figure 3.6). During discharge, the presence of existing Li_2O_2 particles would provide active growth surfaces for the products of O_2 reduction at the cathode. When cycled at C/10 (Figure 3.7a) under this protocol, the stability of the cell is remarkably improved. 551 $mAh\ g^{-1}$ is delivered in the first cycle with efficiency as high as 95% for the first 5 cycles. Even after 50 cycles, the cell can reversibly deliver 487 $mAh\ g^{-1}$ while maintaining an efficiency of 85%. As electrolyte decomposition is not completely eliminated, the cell fails as the efficiency dips below 80% after 58 cycles (not shown). The gradual increase in the voltage over 50 cycles due to minimized parasitic reactions can be observed (Figure 3.6). Under this cycling regime, the higher rate capability

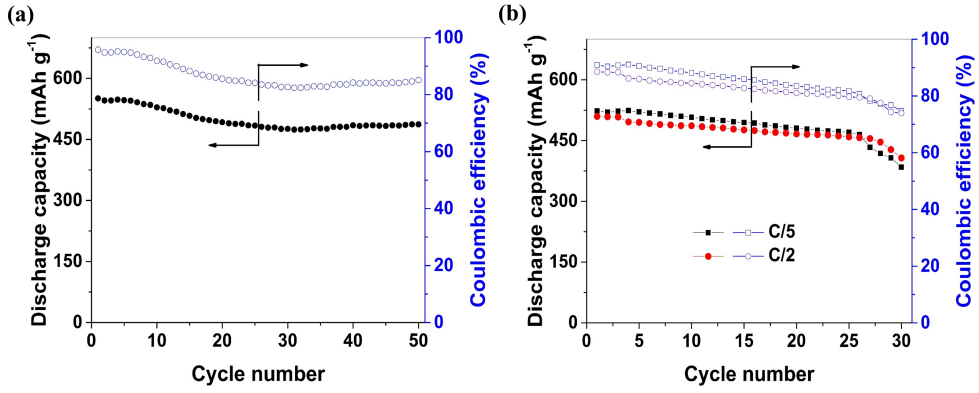

Figure 3.7. Cycle performance under capacity limited charging at (a) C/10 (b) C/5 and C/2 (1C = 1,168 $mA\ g^{-1}$ based on Li_2O_2 mass)

of this cathode architecture was tested. The presence of the intimate contact of Li_2O_2 and CNFs permits good rate capability. As shown in Figure 3.7b, at C/5, 523 $mAh\ g^{-1}$ is obtained at an efficiency of nearly 91% and at C/2, $mAh\ g^{-1}$ with 88.5% efficiency can be obtained. Therefore, it can be observed that the first cycle efficiency reduces at higher rate. The cause of this is evident on seeing the voltage

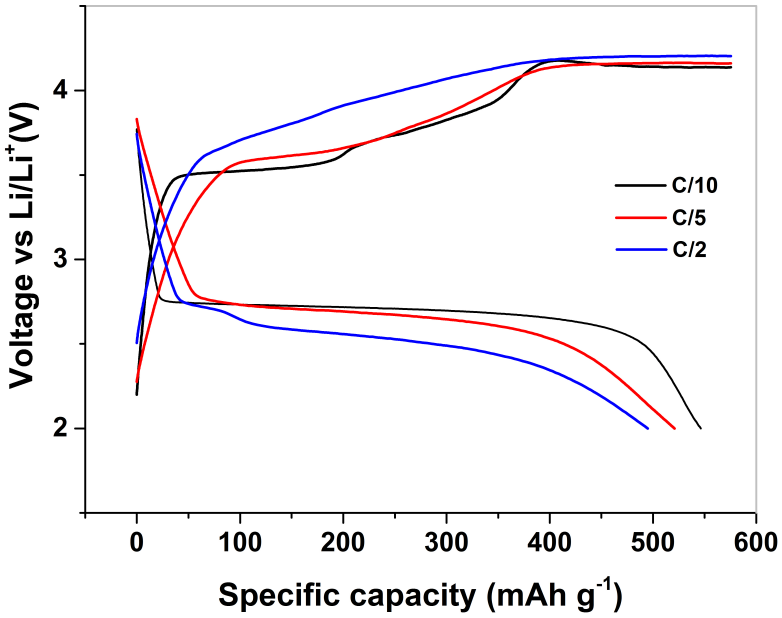

Figure 3.8. Representative voltage profiles of 5th cycle for cells cycled at different C-rates under capacity controlled regime with capacity limited to 50% of theoretical charge capacity of the cathode.(1C = 1,168 $mA\ g^{-1}$ based on Li_2O_2 mass)

profile (Figure 3.8). As the rate increases, the overpotentials broaden with the charge occurring predominantly over 3.8 V in the case of C/2 leading to increased electrolyte decomposition and thus lower efficiency. As a consequence, in both cases, as the efficiency drops below 80%, the cell degrades faster and fails as quickly as 30 cycles. It is also interesting to note that, at C/2 the discharge occurs at 2.5 V. This means that this cathode is capable of delivering high specific power even at higher rates.

3.4 Conclusion

In summary, this work demonstrates an improved closed system Li-O_2 battery wherein chemically synthesized Li_2O_2 nanocrystals intimately embedded in a CNF matrix is capable of operating at lowered overpotentials and showing high rechargeable capacities and prolonged cycle life.[30] On using capacity controlled charging protocol, the parasitic side reactions are significantly minimized leading to remarkably stable cycling of a closed system cell for 50 cycles at C/10. The cell is also able to demonstrate prolonged cycling at rates as high as C/2 while still maintaining a high capacity and good power density. Thus, this synthesis route is feasible for making novel Li_2O_2 based cathode architectures that can provide stable cycling towards the development of Li-O_2 batteries.

3.5 References

[1] P. G. Bruce, S. A. Freunberger, L. J. Hardwick, and J.-M. Tarascon, "Li-O2 and Li-S batteries with high energy storage," *Nature Materials,* vol. 11, pp. 19-29, 2012.

[2] A. C. Luntz and B. D. McCloskey, "Nonaqueous Li–Air Batteries: A Status Report," *Chemical Reviews,* vol. 114, pp. 11721-11750, 2014.

[3] W. Xu, J. Xiao, J. Zhang, D. Wang, and J.-G. Zhang, "Optimization of nonaqueous electrolytes for primary lithium/air batteries operated in ambient environment," *Journal of the Electrochemical Society,* vol. 156, pp. A773-A779, 2009.

[4] M. Leskes, A. J. Moore, G. R. Goward, and C. P. Grey, "Monitoring the Electrochemical Processes in the Lithium–Air Battery by Solid State NMR Spectroscopy," *The Journal of Physical Chemistry C,* vol. 117, pp. 26929-26939, 2013.

[5] V. Viswanathan, K. S. Thygesen, J. S. Hummelshøj, J. K. Nørskov, G. Girishkumar, B. D. McCloskey*, et al.*, "Electrical conductivity in Li2O2 and its role in determining capacity limitations in non-aqueous Li-O2 batteries," *Journal of Chemical Physics,* vol. 135, p. 214704, 2011.

[6] O. Sapunkov, V. Pande, A. Khetan, C. Choomwattana, and V. Viswanathan, "Quantifying the promise of 'beyond'Li–ion batteries," *Translational Materials Research,* vol. 2, p. 045002, 2015.

[7] B. D. McCloskey, C. M. Burke, J. E. Nichols, and S. E. Renfrew, "Mechanistic insights for the development of Li-O2 battery materials: addressing Li2O2 conductivity limitations and electrolyte and cathode instabilities," *Chemical Communications,* vol. 51, pp. 12701-12715, 2015.

[8] Y.-C. Lu, B. M. Gallant, D. G. Kwabi, J. R. Harding, R. R. Mitchell, M. S. Whittingham*, et al.*, "Lithium–oxygen batteries: bridging mechanistic understanding and battery performance," *Energy & Environmental Science,* vol. 6, pp. 750-768, 2013.

[9] M. Noked, M. A. Schroeder, A. J. Pearse, G. W. Rubloff, and S. B. Lee, "Protocols for Evaluating and Reporting Li–O2 Cell Performance," *The Journal of Physical Chemistry Letters,* vol. 7, pp. 211-215, 2016.

[10] T. Ogasawara, A. Débart, M. Holzapfel, P. Novák, and P. G. Bruce, "Rechargeable Li2O2 Electrode for Lithium Batteries," *Journal of the American Chemical Society,* vol. 128, pp. 1390-1393, 2006.

[11] J. R. Harding, Y.-C. Lu, Y. Tsukada, and Y. Shao-Horn, "Evidence of catalyzed oxidation of Li2O2 for rechargeable Li-air battery applications," *Physical Chemistry Chemical Physics,* vol. 14, pp. 10540-10546, 2012.

[12] K. P. C. Yao, Y.-C. Lu, C. V. Amanchukwu, D. G. Kwabi, M. Risch, J. Zhou*, et al.*, "The influence of transition metal oxides on the kinetics of Li2O2 oxidation in Li-O2 batteries: high activity of chromium oxides," *Physical Chemistry Chemical Physics,* vol. 16, pp. 2297-2304, 2014.

[13] Y.-C. Lu, H. A. Gasteiger, M. C. Parent, V. Chiloyan, and Y. Shao-Horn, "The Influence of Catalysts on Discharge and Charge Voltages of Rechargeable Li–Oxygen Batteries," *Electrochemical and Solid-State Letters,* vol. 13, pp. A69-A72, June 1, 2010.

[14] D. Kundu, R. Black, B. Adams, K. Harrison, K. Zavadil, and L. F. Nazar, "Nanostructured Metal Carbides for Aprotic Li–O2 Batteries: New Insights into Interfacial Reactions and Cathode Stability," *The Journal of Physical Chemistry Letters,* vol. 6, pp. 2252-2258, 2015.

[15] S. Meini, N. Tsiouvaras, K. U. Schwenke, M. Piana, H. Beyer, L. Lange*, et al.*, "Rechargeability of Li–air cathodes pre-filled with discharge products using an ether-based electrolyte solution: implications for cycle-life of Li–air cells," *Physical Chemistry Chemical Physics,* vol. 15, pp. 11478-11493, 2013.

[16] H. Beyer, S. Meini, N. Tsiouvaras, M. Piana, and H. Gasteiger, "Thermal and electrochemical decomposition of lithium peroxide in non-catalyzed carbon cathodes for Li–air batteries," *Physical Chemistry Chemical Physics,* vol. 15, pp. 11025-11037, 2013.

[17] A. Bhargav and Y. Fu, "Lithium Peroxide-Carbon Composite Cathode for Closed System Li-O2 Batteries," *Journal of The Electrochemical Society,* vol. 162, pp. A1327-A1333, 2015.

[18] C. V. Amanchukwu, J. R. Harding, Y. Shao-Horn, and P. T. Hammond, "Understanding the Chemical Stability of Polymers for Lithium–Air Batteries," *Chemistry of Materials,* vol. 27, pp. 550-561, 2015.

[19] J. Khosravi, *Production of Lithium Peroxide and Lithium Oxide in an Alcohol Medium*, Ph.D. dissertation, McGill University Montreal, Canada, 2007.

[20] C. M. Burke, V. Pande, A. Khetan, V. Viswanathan, and B. D. McCloskey, "Enhancing electrochemical intermediate solvation through electrolyte anion selection to increase nonaqueous Li–O2 battery capacity," *Proceedings of the National Academy of Sciences of the United States of America,* vol. 112, pp. 9293-9298, 2015.

[21] B. D. McCloskey, A. Valery, A. C. Luntz, S. R. Gowda, G. M. Wallraff, J. M. Garcia*, et al.*, "Combining Accurate O2 and Li2O2 Assays to Separate Discharge and Charge Stability Limitations in Nonaqueous Li–O2 Batteries," *The Journal of Physical Chemistry Letters,* vol. 4, pp. 2989-2993, 2013.

[22] M. M. Ottakam Thotiyl, S. A. Freunberger, Z. Peng, and P. G. Bruce, "The carbon electrode in nonaqueous Li–O2 cells," *Journal of the American Chemical Society,* vol. 135, pp. 494-500, 2012.

[23] S. Xu, S. Lau, and L. A. Archer, "CO 2 and ambient air in metal–oxygen batteries: steps towards reality," *Inorganic Chemistry Frontiers,* vol. 2, pp. 1070-1079, 2015.

[24] S. Huang, W. Fan, X. Guo, F. Meng, and X. Liu, "Positive Role of Surface Defects on Carbon Nanotube Cathodes in Overpotential and Capacity Retention of Rechargeable Lithium–Oxygen Batteries," *ACS Applied Materials & Interfaces,* vol. 6, pp. 21567-21575, 2014.

[25] K. Takechi, T. Shiga, and T. Asaoka, "A Li-O2/CO2 battery," *Chemical Communications,* vol. 47, pp. 3463-3465, 2011.

[26] H.-K. Lim, H.-D. Lim, K.-Y. Park, D.-H. Seo, H. Gwon, J. Hong*, et al.*, "Toward a Lithium–"Air" Battery: The Effect of CO2 on the Chemistry of a Lithium–Oxygen Cell," *Journal of the American Chemical Society,* vol. 135, pp. 9733-9742, 2013.

[27] Y. S. Mekonnen, J. M. Garcia-Lastra, J. S. Hummelshøj, C. Jin, and T. Vegge, "Role of Li2O2@ Li2CO3 Interfaces on Charge Transport in Nonaqueous Li–Air Batteries," *The Journal of Physical Chemistry C,* vol. 119, pp. 18066-18073, 2015.

[28] A. Dunst, V. Epp, I. Hanzu, S. Freunberger, and M. Wilkening, "Short-range Li diffusion vs. long-range ionic conduction in nanocrystalline lithium peroxide Li 2 O 2—the discharge product in lithium-air batteries," *Energy & Environmental Science,* vol. 7, pp. 2739-2752, 2014.

[29] N. B. Aetukuri, B. D. McCloskey, J. M. García, L. E. Krupp, V. Viswanathan, and A. C. Luntz, "Solvating additives drive solution-mediated electrochemistry and enhance toroid growth in non-aqueous Li–O2 batteries," *Nature chemistry,* vol. 7, pp. 50-56, 2015.

[30] A. Bhargav and Y. Fu, "Chemically synthesized lithium peroxide composite cathodes for closed system Li–O2 batteries," *Chemical Communications,* vol. 52, pp. 5678-5681, 2016.

4. GRAPHITE-POLYSULFIDE FULL CELL WITH DME-BASED ELECTROLYTE

4.1 Introduction

The demand for energy consumption by mankind is ever increasing due to rapid growth and accessibility of technology by the masses. This has led to our dependence on fossil fuels like coal and petroleum. Fortunately, sulfur, one of the promising cathode materials for inexpensive high energy density lithium batteries arises as a by-product of petroleum refining.[1] Its abundant, benign nature combined with the ability of lithium-sulfur (Li-S) cells to provide a theoretical specific capacity of 1,672 $mAh\ g^{-1}$ and specific energy of 2,600 $Wh\ kg^{-1}$ makes it an attractive cathode material.[2] With high promises come significant challenges in utilizing this material effectively towards commercialization. The significant ones being the low conductivity of sulfur and lithium sulfide, the shuttle effect caused by the mobile intermediate polysulfides, and the volume changes upon cycling in the cathode.[2-4] In recent years, most of the research efforts have been focused to tackle issues at the cathode side. The pure lithium metal used in the cell also poses crucial challenges in the development of Li-S systems. Chief among them being the formation of Li dendrites and mossy deposits on the Li anode,[5, 6] presence of excess lithium which assists the shuttle effect,[7] and low Coulombic efficiency associated with Li metal deposition and stripping which leads to short cycle life.[5] To overcome the shortcomings on the anode side different non-Li metal anodes have been tested such as graphite,[8-11] hard carbon,[12] silicon,[13, 14] tin,[15] and other alloys.[8] Although non-lithium anodes prevent Li-dendrite formation and increase Coulombic efficiency at the anode side, it is imperative that a compatible electrolyte that can form a stable solid electrolyte interphase (SEI) and promote high anode capacity is used. The specific capacity

provided by the graphite anode while using the common electrolyte of 1 M LiTFSI in DME/DOL is much lower than the carbonate electrolyte for Li-ion batteries, i.e. 1 M $LiPF_6$ in EC/DEC.[11] This provides the motivation to develop alternative electrolytes that work with graphite while utilizing higher anode capacity that facilitates higher energy density.

In this regard, recent work on high concentration electrolytes have shown to offer stable Li intercalation into graphite.[16] Not only this, high electrolyte concentration effectively suppresses the lithium polysulfide shuttle effect when coupled with Li-S batteries.[17, 18] In this work, we have incorporated a new high concentration electrolyte based on a combination of 3 M lithium bis(fluorosulfonyl)imide (LiFSI, $LiN(SO_2F)_2$) and 1 M lithium bis(trifluoromethane sulfonyl) imide (LiTFSI, $LiN(SO_2CF_3)_2$) in 1,2-dimethoxyethane (DME) as the solvent. This electrolyte uses the beneficial effects of both the LiFSI and LiTFSI salts while supporting Li intercalation at the anode and suppressing polysulfide shuttle from the cathode.[19-21] Full cells were made with a novel lithium polysulfide cathode and MCMB based anode. The cells exhibit good cycle performance and high rate capability. The morphological changes at both the cathode and anode before and after cycling were studied to better understand the lithium-metal-free Li-S full cells.

4.2 Experimental

4.2.1 Anode Preparation

A slurry containing 80 wt.% MesoCarbon MicroBeads (MCMB, MTI corp.), 10 wt.% Super C65 (conductive carbon black, Timcal), and 10 wt.% polyvinylidene fluoride (PVdF, Kureha Battery Materials Japan Co., Ltd.) with N-methyl-2-pyrrolidone (NMP, Acros Organics) solvent was cast on Toray carbon paper (TGP-H-090, Fuel Cell Earth LLC) using a doctor blade. The electrode was dried overnight at 100°C. The electrode sheet was punched into approximately 1 cm^2 discs with MCMB loading of about 1.4 $mg\ cm^{-2}$ and used as the anode. In this MCMB-carbon paper (MCMB-

CP) hybrid anode, lithium storage capacity comes from both the MCMB and carbon paper. 50% of the weight of the carbon paper disc (∼12.4 mg) consists of graphitic carbon,[22] the mass of which is included in the specific capacity calculation.

4.2.2 Cathode Preparation

The lithium polysulfide solution was prepared by dissolving stoichiometric amounts of lithium sulfide (Li_2S, Sigma Aldrich) and sublimed sulfur (S, Fisher scientific) to form 0.25 M Li_2S_6 (corresponding to 1.5 M sulfur) in methanol. Also, 0.75 M Li_2S_6 solution in ethanol was prepared to develop the higher loading cathode. The cathode consisted of 1 cm^2 discs of commercial multiwall carbon nanotube (MWCNT) paper or buckypaper (NTL composites) to which 20 μL of 0.25 M Li_2S_6 solution was added and let to dry overnight to yield the solid lithium polysulfide cathode containing 1.0 mg of sulfur, which was primarily used in this study. 30 μL of 0.75 M solution was used to prepare the high loading cathode containing 4.3 mg of sulfur.

4.2.3 Electrochemical Testing

The primary electrolyte used in this study consists of 3 M lithium bis(fluorosulfonyl) imide (LiFSI, Oakwood Chemical) and 1 M lithium bis(trifluoromethanesulfonyl) imide (LiTFSI, Sigma Aldrich) in 1,2-dimethoxyethane (DME, Sigma Aldrich) as the solvent. 1 M LiTFSI in DME and 1,3-dioxolane (DOL, Sigma Aldrich) in 1:1 v/v ratio as an electrolyte and commercial Li-ion battery electrolyte, i.e. 1 M $LiPF_6$ in ethylene carbonate/diethyl carbonate (EC/DEC, 1:1 v/v, Novolyte) were used in comparison studies. Half-cell tests were carried out using CR2032 type coin cells with the anode/cathode discs, 30 μL of electrolyte, Celgard 2400 separator and lithium metal disc as the counter and reference electrode. The cells were cycled between 2 - 0.01 V for anode tests and between 3.0 - 1.8 V for cathode tests at the appropriate C-rate (1 C corresponding to 372 $mA\ g^{-1}$ graphite for the anode and 1,672 $mA\ g^{-1}$ sulfur for the cathode). For full cells, the MCMB-CP anode was pre-lithiated using

a half-cell at C/15 and the lithiated anode was extracted, washed with neat DME, and dried in the glovebox atmosphere before being used as an anode. The full cell was made by coupling the polysulfide cathode with the MCMB-CP anode. Full cells were cycled at the appropriate C-rate (1 C corresponding to 1,672 $mA\ g^{-1}$ sulfur in the cathode) between 2.8 - 1.85 V. Cyclic voltammetry (CV) was performed on a Bio-Logic VSP potentiostat between 2.8 - 1.8 V at a scanning rate of 0.1 $mV\ s^{-1}$.

4.2.4 Characterization

Structure and morphology change was observed using scanning electron microscopy (SEM) performed on a JEOL JSM-7800F field emission scanning electron microscope equipped with energy-dispersive X-ray spectroscopy (EDX). SEM samples were washed using DME solvent and dried before being mounted inside the glovebox. The samples were transferred using an argon-filled sealed container. X-Ray Diffraction (XRD) studies used a Bruker D8 Discover diffractometer with Cu Kα radiation source of wavelength 1.54184 Å for 2θ between 20° and 80° at a scan rate of $1.25°min^{-1}$. XRD samples were prepared similar to SEM samples and covered with a Kapton film to prevent any exposure to air.

4.3 Results and Discussion

4.3.1 Anode and Electrolyte

The anode used in the full cell consists of MCMB graphite embedded in a matrix of carbon fibers of the carbon paper to form the MCMB-CP hybrid anode. Figure 4.1a shows the SEM image of the top surface of the anode. MCMB particles are deeply covered in super C65 thus ensuring good electrical contact into the graphite. The SEM image (Figure 4.1b) of the anode cross-section shows the MCMB-super C65 composite is present through the depth of the carbon fiber of the carbon paper. The filled pores of the crisscrossed carbon fibers ensure abundant electron transfer

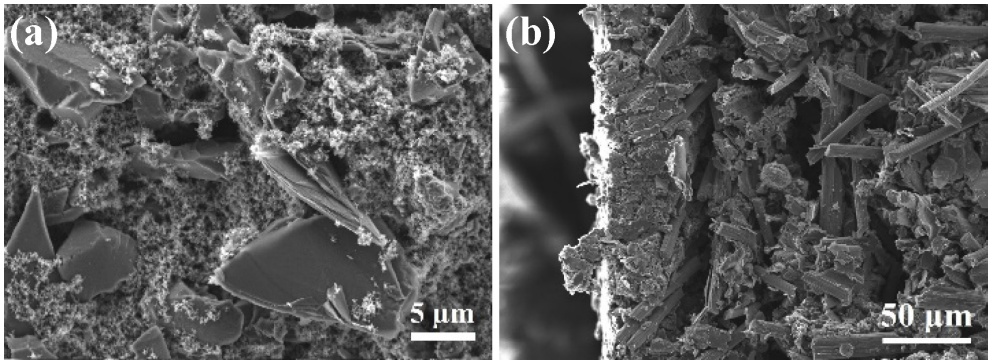

Figure 4.1. SEM images of the MCMB-CP anode showing (a) its face and (b) its cross-section.

pathways while reducing the porosity of the anode which could reduce polysulfide retention due to shuttle effect.

XRD investigation of the pristine anode (Figure 4.2a) shows a distinctive sharp peak at 26.4° corresponding to the (002) plane of the graphite present in both MCMB and the carbon paper. There is also a broad slope at about 26° which arises due to the non-graphitic carbon fibers present in the carbon paper. On electrochemical lithiation of this anode, the peak shifts to 24.5° owing to the increase in the graphite interlayer spacing due to lithium intercalation. On de-intercalation, the graphite returns to its original configuration thus showing the reversible lithium intercalation and de-intercalation supported by the 3 M LiFSI/1 M LiTFSI in DME electrolyte.

High concentration LiFSI based electrolytes have shown stable lithium intercalation.[16] But, LiFSI-based electrolyte shows unfavorable performance with sulfur cathode at room temperature.[21] However, the addition of a similar salt, namely, LiTFSI can stabilize the electrolyte due to common-ion effect.[19, 20] Thus, this unique combination of 3 M LiFSI and 1 M LiTFSI has been used in this study to accommodate both highly reversible lithium intercalation behavior offered by LiFSI and the stability with sulfur cathode provided by LiTFSI while utilizing DME alone as the electrolyte solvent.

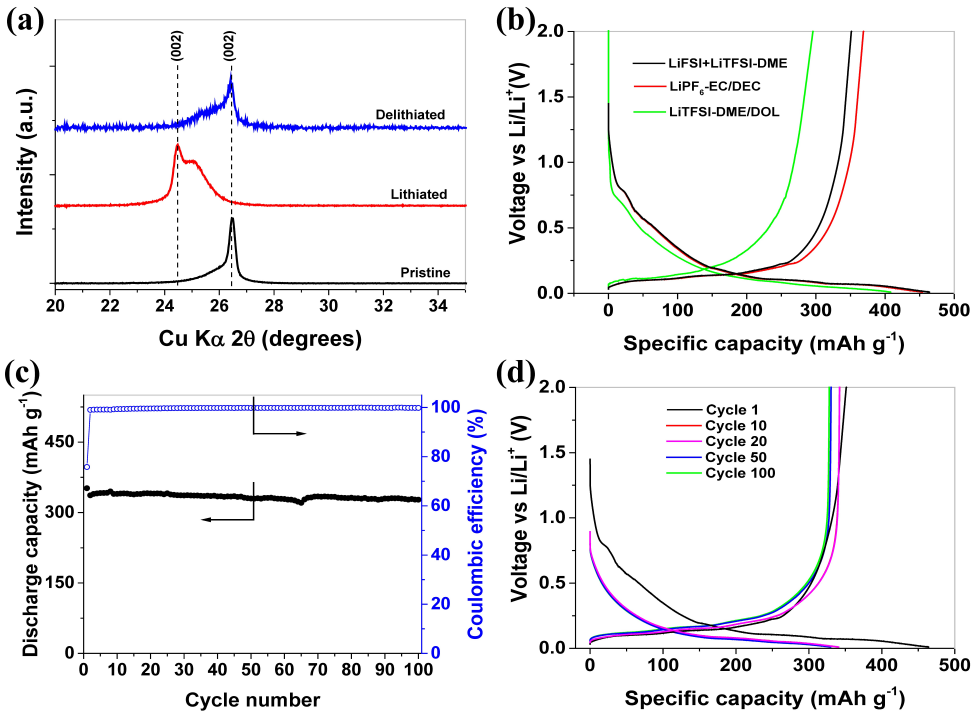

Figure 4.2. (a) XRD showing the intercalation behaviour of MCMB-CP anode with 3 M LiFSI + 1 M LiTFSI in DME electrolyte, (b) first cycle performance comparing the anode performance under different electrolytes, (c) cycle life of the MCMB-CP anode with DME electrolyte along with the corresponding voltage profiles in (d). The cells were cycled at C/10 (1C = 372 $mA\ g^{-1}$, based on the mass of graphite in the whole electrode).

To compare the performance of this newly developed electrolyte with the commercial Li-ion battery electrolyte which is known to exhibit high capacity and reversibility and the electrolyte commonly used in Li-S studies, including full cell studies,[9, 12] half cells with the MCMB-CP anode were tested. The first cycle performance shown in Figure 4.2b uses reversible specific capacity delivered by the anode as a measure of the effectiveness these electrolytes. Higher specific capacity equates to lower amount of graphite required to support the capacity delivered by sulfur cathode, thus improving the specific energy of the system. It is apparent that the best performance is provided by the carbonate based electrolyte. However, it is incompatible with sulfur cathode.[23] Thus, among the ether based electrolytes, the one containing 3 M LiFSI

and 1 M LiTFSI in DME alone shows a much higher reversible capacity of 350 $mAh\ g^{-1}$ over the commonly used DME/DOL based electrolyte which shows less than 300 $mAh\ g^{-1}$, making it a more suitable choice for Li-S full cells. The compatibility and longevity of the MCMB-CP anode was further tested in this electrolyte. The DME electrolyte shows excellent reversibility over 100 cycles as evidenced in Figure 4.2c. Beyond the 1st cycle, the Coulombic efficiency is about 99.8% establishing the stability of the SEI layer and that of the electrolyte with the anode. The specific capacity delivered by the cell drops to about 340 $mAh\ g^{-1}$ in the second cycle, but stabilizes and still yields 327 $mAh\ g^{-1}$ after 100 cycles. The voltage profile of the anode in Figure 4.2d with the first discharge exhibits a short plateau at 0.8 V owing to the SEI layer formation. It also clearly shows the multi-step lithium intercalation into graphite.[24] On lithium extraction, a reversible capacity of 350 $mAh\ g^{-1}$ is obtained with a Coulombic efficiency of about 75% due to irreversible loss in the SEI formation. On further cycling, The Li insertion voltage settles to 0.09 V from cycle 10 to 100. Li extraction occurs at 0.16 V at the 10th cycle which increases to about 0.18 V by the 100th cycle. Thus, the combination of 3 M LiFSI and 1 M LiTFSI in DME yields a highly compatible electrolyte with the graphite anode. It has been shown that graphitic carbon paper can work as an effective anode in carbonate electrolyte.[22, 25] In the MCMB-CP anode, the capacity contribution from the carbon paper is about 2.18 mAh and that of MCMB is 0.48 mAh thus providing a combined capacity of 2.66 mAh. Therefore, based on the sulfur in the cathode, there would be about 65% excess lithium on the anode providing sufficient capacity balance to operate a full cell while utilizing the full potential of sulfur.

4.3.2 Polysulfide Cathode

A novel approach to deposit solid lithium polysulfide in the cathode was developed in this work. It has been shown that polysulfide dissolved in the electrolyte works as a highly reversible sulfur source in a Li-S battery.[26] It has also been shown that

such a system is ideal for developing high sulfur loading cathodes.[27] However, this approach limits the energy density as a large amount of electrolyte is required to deliver the sulfur. This can be circumvented by using the solvent evaporation technique utilized in this work. In this method, lithium polysulfide solution is prepared in a low boiling point media such as alcohol and deposited into a conductive substrate such as MWCNT paper and dried to remove the solvent leaving the polysulfide evenly distributed within the cathode.

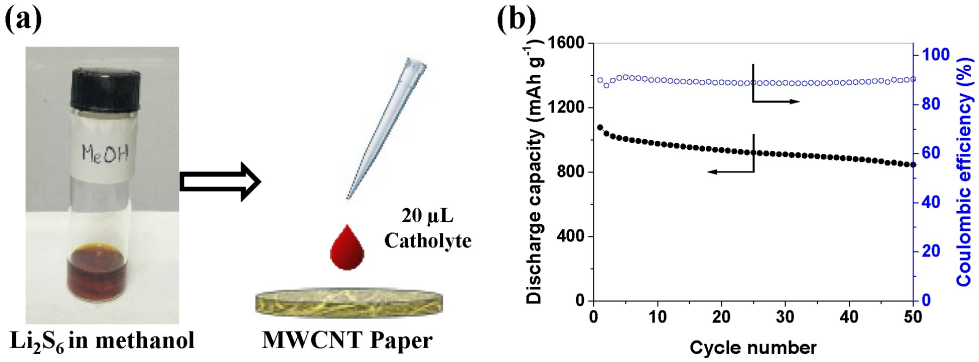

Figure 4.3. (a) Schematic showing the cathode preparation technique through lithium polysulfide deposition on MWCNT paper. (b) Cycling performance of high loading sulfur cell with 4.3 mg sulfur deposited on MWCNT paper. The cell was cycled at C/10 (1C corresponding to 1,672 $mA\ g^{-1}$ sulfur for the cathode).

This process is outlined in the Schematic in figure 4.3a which shows the homogeneous 0.25 M Li_2S_6 solution in methanol and illustrates the cathode preparation technique. Such an approach also has the advantage of introducing extra lithium in the cathode thus minimizing the amount of lithium required in the anode. We utilized both 0.25 M and 0.75 M solutions of Li_2S_6 to introduce polysulfide into the cell to demonstrate the viability of utilizing this technique to develop high polysulfide loading cathodes. The performance of the high loading cathode is shown in Figure 4.3b. For the purpose of full cell study, the lower loading cathode was utilized due to the ease of fabrication of the anode with a lower loading of graphite at lab scale.

However, this approach is scalable and can be utilized with higher loading of active materials on both the anode and cathode.

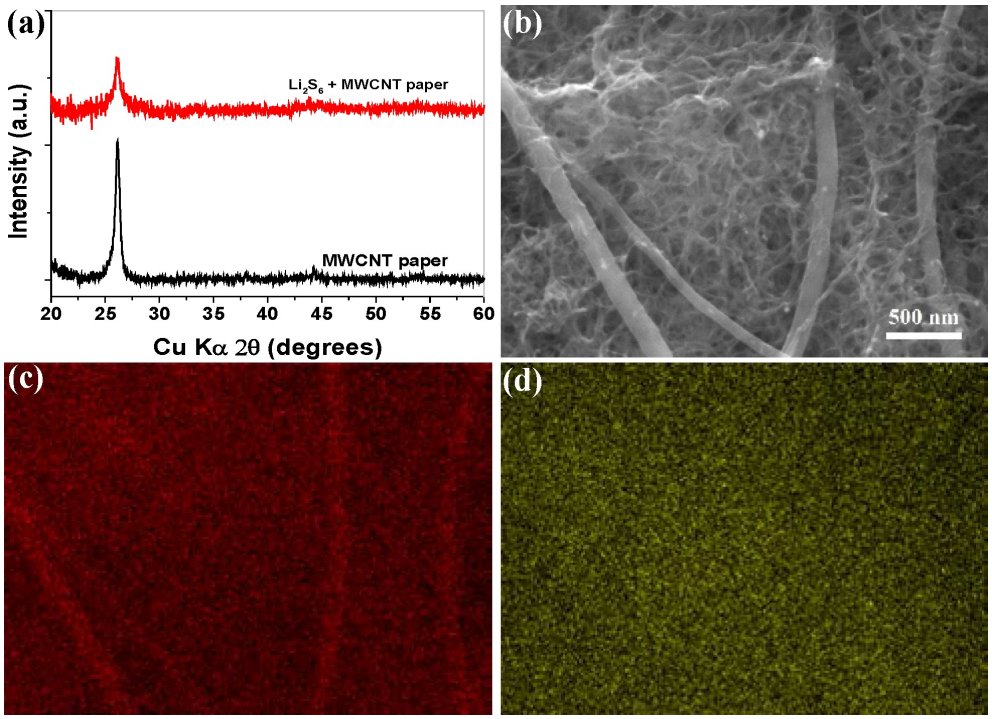

Figure 4.4. (a) XRD analysis of the polysulfide indicating amorphous deposits of polysulfide on the MWCNT paper, (b) SEM micrograph of the cathode along with EDX mapping of (c) carbon and (d) sulfur showing uniform coating of polysulfides throughout the cathode.

The absence of elemental sulfur or lithium sulfide in the cathode thus prepared was verified by XRD in Figure 4.4a. The XRD of the cathode shows diminished peaks of the MWCNT paper thus proving that the cathode consists of an amorphous, conformal coating of lithium polysulfides. This was further confirmed through scanning electron microscopy (SEM). The SEM micrograph (Figure 4.4b) shows no distinct particles on the carbon network of the cathode. However, what appears to be a conformal coating of the lithium polysulfide species on the carbon is clearly observed. It is also possible that polysulfide species is absorbed by the pores of carbon nanotubes. The EDX mapping of carbon (Figure 4.4c) and sulfur (Figure 4.4d) confirm the uniform coating of polysulfide species in the cathode.

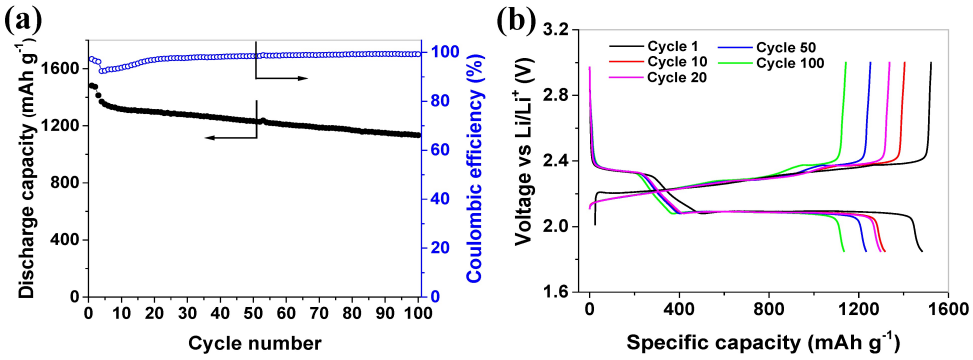

Figure 4.5. Performance of the polysulfide cathode with DME electrolyte showing (a) cycle life and (b) voltage profile of the same. The cells were cycled at C/10 (1C = 1,672 $mA\ g^{-1}$, based on the mass of sulfur in the cathode).

Half-cells were made with this cathode to examine its performance with the DME based electrolyte. The cycle life of the cell when cycled at C/10 is shown in Figure 4.5a. During the initial cycles, the capacity drops from 1,481 $mAh\ g^{-1}$ in the first cycle to $mAh\ g^{-1}$ in the 4th cycle. The Coulombic efficiency drops to 93% in the same interval. This loss is probably due to minor polysulfide shuttle before the cell stabilizes. Beyond 20 cycles, electrochemical stability improves with the Coulombic efficiency reaching over 98%. After 100 cycles, the cell manages to deliver over $mAh\ g^{-1}$ showing remarkable stability despite the absence of additives such as $LiNO_3$. This demonstrates that the cathode prepared through this technique is robust in retaining most of the polysulfide generated during cell cycling within the pores of the cathode thus offering stable performance. The voltage profile of the cathode during first discharge shows the conversion of the high-order polysulfides (Li_2S_x, $6 \geq x \leq 8$) to Li_2S_4 above 2.1 V and its conversion to intermediate polysulfides (Li_2S_x, $2 \geq x \leq 4$) at 2.1 V and lithium sulfide (Li_2S) at the end of discharge (Figure 4.5b). The following recharge converts the Li_2S to high-order polysulfides/elemental sulfur through the reversal of the discharge process. The charge process is able to reach completion beyond 2.4 V without leading to severe polysulfide shuttle.

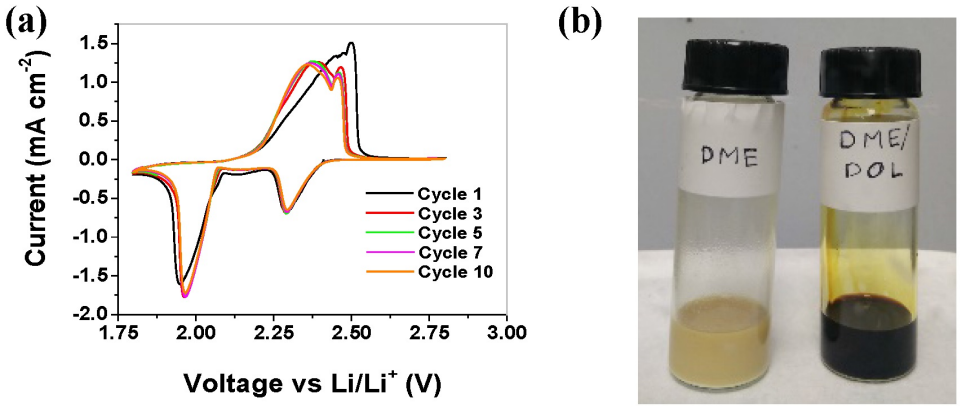

Figure 4.6. (a) Cyclic voltammogram of the polysulfide cathode showing its high reversibility. The scan rate is $mV\ s^{-1}$. (b) Optical image demonstrating the relative insolubility of lithium polysulfide in the DME electrolyte used in this work (left) and the ease of lithium polysulfide formation in the conventional DME/DOL electrolyte. To prepare this, stoichiometric amounts of Li_2S and elemental sulfur was stirred in the electrolytes for 24 h.

This highly reversible cycling is also captured by the cyclic voltammogram in Figure 4.6a. The continuous overlap of the peaks confirms the stability of the lithium polysulfide cathode with the new electrolyte. The high salt concentration of this electrolyte leads to higher viscosity thus inhibiting polysulfide dissolution and migration to the anode side.[17, 21] This capability of the electrolyte is demonstrated by its inability to form soluble polysulfide species on stirring of stoichiometric quantities of Li_2S and elemental S in a vial containing the electrolyte (Figure 4.6b). In comparison, as in Figure 4.6b, the common DME/DOL electrolyte is able to easily form polysulfide solution.

4.3.3 Full Cell Performance

The excellent cycling stability offered by the cathode affords its use in the full cell setup. When coupled with the lithiated MCMB-CP anode and cycled at C/10, the cycling performance in Figure 7.7a is observed. The initial formation cycles

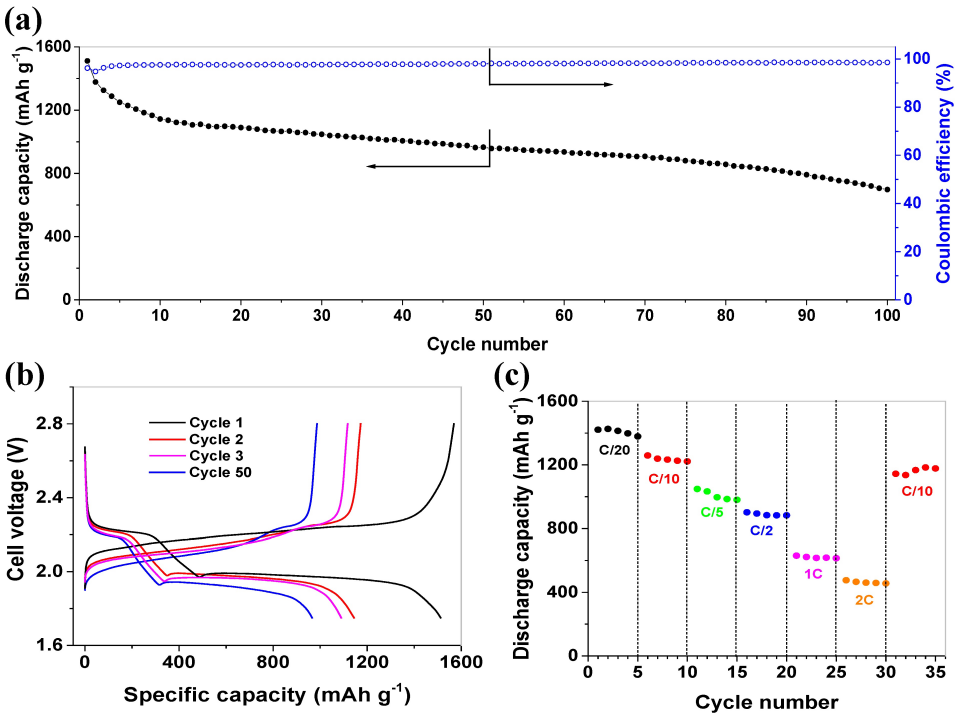

Figure 4.7. (a) Cycling performance of the full cell at C/10 with its corresponding (b) voltage profile and (c) rate performance of the cathode. The cells were cycled at C/10 (1C = 1,672 $mA\ g^{-1}$, based on the mass of sulfur in the cathode).

results in capacity decay from over 1,500 $mAh\ g^{-1}$ to about 1,150 $mAh\ g^{-1}$ as the anode and cathode performance stabilizes. Post stabilization, the full cell exhibits stable performance with Coulombic efficiency over 97%. At the end of 100 cycles, about 700 $mAh\ g^{-1}$ of the capacity is retained. In the first cycle (Figure 7.7b), as the cell discharges, 65% excess lithium is present in the anode and thus operates at a lower potential ensuring high cell operating voltage. The high Li extraction efficiency at the anode results in a high first discharge capacity of over 1,500 $mAh\ g^{-1}$. The first cycle Coulombic efficiency is over 96%. As the cycling progresses, both the discharge potential and the charge potential gradually lower, reducing the cell operating voltages. This is due to the consumption of lithium as the cycling progresses. This will be further discussed in the post-mortem analysis section.

The full cell was tested using rates varying from C/20 to 2C to determine the reversible sulfur utilization at different rates with 1C corresponding to a current of 1,672 $mA\ g^{-1}$ sulfur (Figure 7.7c). At C/20, a high reversible capacity of about $mAh\ g^{-1}$ g-1 is delivered by the cell. While cycling at C/10, the cell delivers over $mAh\ g^{-1}$. At higher rates of C/5, C/2, 1C, and 2C, 1000 $mAh\ g^{-1}$, 880 $mAh\ g^{-1}$, 610 $mAh\ g^{-1}$, and 460 $mAh\ g^{-1}$, respectively, can be extracted from the cell. On returning to C/10, the cell is able to recover to the initial capacity level of 1,180 $mAh\ g^{-1}$.This demonstrates excellent electrochemical reversibility of the cathode, enhanced Li diffusion through the anode and fast ion transport through the electrolyte. Thus, this full cell is able to deliver high capacities even under high rates.

4.3.4 Post-Mortem Analysis

The substrate used in the cathode to deposit the polysulfide was commercial MWCNT paper that was used without any treatment. The primary contributor to the longevity of the cell is the ability of the MWCNT paper to contain the polysulfides. The cathode recovered from the cell after 100 cycles in the charged state (Figure 4.8a and b) is compared with that of the pristine cathode (Figure 4.8c and d). It is evident that, after 100 cycles, the MWCNT structure of the cathode still exhibits mechanical robustness and is able to accommodate the volume change occurring in the cathode. It also shows that the sulfur species is uniformly deposited and retained by the carbon network. Although the electrolyte diminishes polysulfide solubility, some amount of it still diffuses over extended time which can be evidenced from the cycled anode. Comparison is made between an anode extracted from a half cell after first cycle (Figures 4.9a, b, and c) and the anode extracted from a full cell after 100 cycles (Figures 4.9d, e, and f). The EDX map of both oxygen species (Figures 4.9b and e) and sulfur species (Figures 4.9c and f) shed light on the two important reactions occurring at the anode, namely, SEI layer formation involving oxygen species arising from DME and the salts and sulfur migration due to shuttle effect. After first cycle,

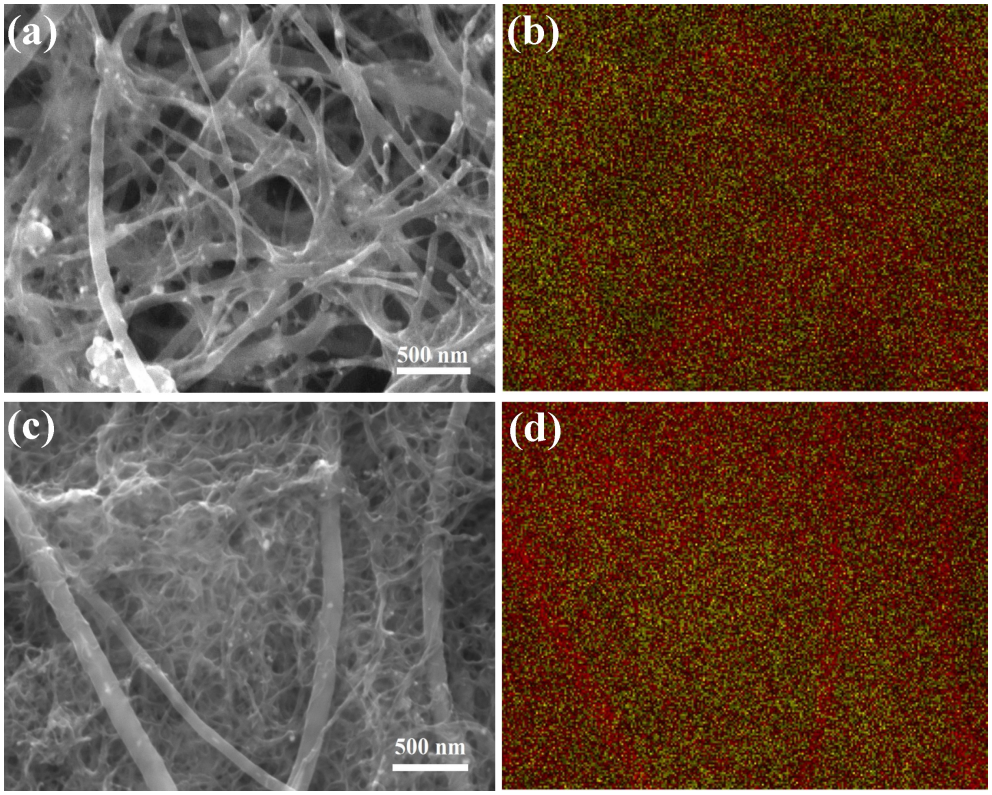

Figure 4.8. SEM image of the cathode (a) extracted after 100 cycles from a full cell accompanying its EDX mapping in (b) along with (c) as prepared cathode with its EDX mapping in (d). Red represents carbon in the EDX map and yellow represents sulfur.

the anode shows a uniform, invisible formation of SEI on the surface of the MCMB particle as evidenced from the uniform distribution of oxygen species on graphite surface. There is almost no sulfur observed barring a small amount on the super C65 particles arising out of the decomposition of salts. This shows the formation of a uniform, robust SEI on the anode. In the cycled anode appears a distinct layer of deposits on both the MCMB and super C65 surface. The elemental mapping provides evidence on the nature of the deposit. It is most likely composed of sulfur species which on migration from the cathode, were reduced on the anode surface and deposited there. This process corrodes the SEI layer leading to its reformation through

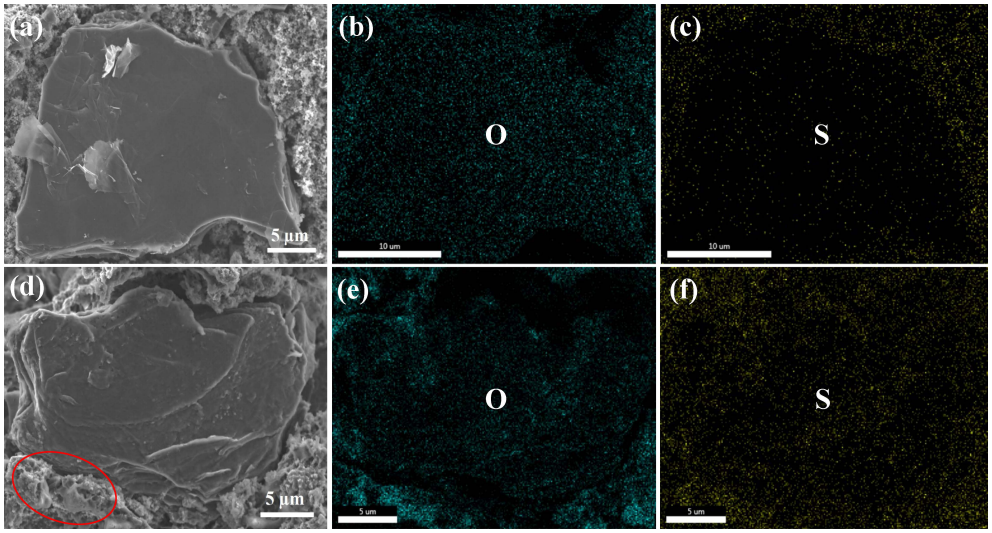

Figure 4.9. Post-mortem analysis of a MCMB-CP anode through (a) SEM micrograph along with EDX map of oxygen (b) and sulfur species (c) extracted from a half-cell compared with those of an anode from a cycled full cell (d), (e), and (f). Anodes were washed with DME solvent prior to analysis. The highlighted portion indicates insoluble sulfur species deposited on the anode.

electrolyte decomposition. The high sulfur concentration in the deposit highlighted in Figure 4.9d supports this hypothesis.

Therefore, the polysulfide shuttle, although not severe, leads to the loss of capacity over cycles. As there still exists a minor shuttle effect, the migrating polysulfides slowly consume lithium at the anode and form deposits of Li_2S_2/Li_2S. As ten or more moles of Li is required per mole of Li_2S_6 (or higher order) that migrate to the anode side, the excess lithium present in the anode depletes fast leading to the operation of the anode at higher potential. This reduces the cell voltage as observed in Figure 4.5b. The performance of such a system could be enhanced by modification of the polysulfide host such as functionalization of CNT, [28] modification of current collectors, [29] use of other host materials such as graphene, [30] ordered carbon, [31] and other non-carbonaceous hosts to contain lithium polysulfides in the cathode. [32] Lithium sulfide cathodes with low overpotentials can also be used. [33]

4.4 Conclusion

A major factor slowing the progress of Li-S batteries towards commercialization is the lack of a viable alternative to the lithium metal anode. The development of electrolytes that can provide stable, long term cycling with non-lithium anodes such as graphite while maintaining compatibility with sulfur cathode is a viable direction towards the progress of Li-S batteries. In this work, we have utilized a graphitic anode consisting of MCMB embedded in carbon paper that demonstrates stable lithium intercalation and de-intercalation through the formation of a robust SEI while using 3 M LiFSI and 1 M LITFSI in DME as the electrolyte. This unique electrolyte combination enhances the compatibility with sulfur cathode. We also report a novel technique for solid lithium polysulfide introduction into a carbon current collector. On coupling this cathode with the graphitic anode in the new electrolyte system, a stable, high performance full cell is obtained. This work demonstrates the viability of utilizing this approach of cathode and anode design to increase active material loading and cycle life through material optimization which can work in tandem with the new electrolyte to make a high energy density and long life Li-S full cells.[34]

4.5 References

[1] J. Lim, J. Pyun, and K. Char, "Recent Approaches for the Direct Use of Elemental Sulfur in the Synthesis and Processing of Advanced Materials," *Angewandte Chemie International Edition,* vol. 54, pp. 3249-3258, 2015.

[2] A. Manthiram, Y. Fu, S.-H. Chung, C. Zu, and Y.-S. Su, "Rechargeable lithium–sulfur batteries," *Chemical Reviews,* vol. 114, pp. 11751-11787, 2014.

[3] A. Manthiram, Y. Fu, and Y.-S. Su, "Challenges and prospects of lithium–sulfur batteries," *Accounts of Chemical Research,* vol. 46, pp. 1125-1134, 2012.

[4] S. S. Zhang, "Liquid electrolyte lithium/sulfur battery: fundamental chemistry, problems, and solutions," *Journal of Power Sources,* vol. 231, pp. 153-162, 2013.

[5] H. Kim, G. Jeong, Y.-U. Kim, J.-H. Kim, C.-M. Park, and H.-J. Sohn, "Metallic anodes for next generation secondary batteries," *Chemical Society Reviews,* vol. 42, pp. 9011-9034, 2013.

[6] D. Lu, Y. Shao, T. Lozano, W. D. Bennett, G. L. Graff, B. Polzin*, et al.*, "Failure Mechanism for Fast-Charged Lithium Metal Batteries with Liquid Electrolytes," *Advanced Energy Materials,* vol. 5, p. 1400993, 2015.

[7] D. Aurbach, E. Pollak, R. Elazari, G. Salitra, C. S. Kelley, and J. Affinito, "On the surface chemical aspects of very high energy density, rechargeable Li–sulfur batteries," *Journal of the Electrochemical Society,* vol. 156, pp. A694-A702, 2009.

[8] R. Cao, W. Xu, D. Lv, J. Xiao, and J.-G. Zhang, "Anodes for Rechargeable Lithium-Sulfur Batteries," *Advanced Energy Materials,* vol. 5, p. 1402273, 2015.

[9] M. Agostini, B. Scrosati, and J. Hassoun, "An Advanced Lithium-Ion Sulfur Battery for High Energy Storage," *Advanced Energy Materials,* vol. 5, p. 1500481, 2015.

[10] S. Zheng, Y. Chen, Y. Xu, F. Yi, Y. Zhu, Y. Liu*, et al.*, "In situ formed lithium sulfide/microporous carbon cathodes for lithium-ion batteries," *ACS Nano,* vol. 7, pp. 10995-11003, Dec 23 2013.

[11] D. Lv, P. Yan, Y. Shao, Q. Li, S. Ferrara, H. Pan*, et al.*, "High performance Li-ion sulfur batteries enabled by intercalation chemistry," *Chemical Communications,* vol. 51, pp. 13454-13457, 2015.

[12] J. Brückner, S. Thieme, F. Böttger-Hiller, I. Bauer, H. T. Grossmann, P. Strubel*, et al.*, "Carbon-Based Anodes for Lithium Sulfur Full Cells with High Cycle Stability," *Advanced Functional Materials,* vol. 24, pp. 1284-1289, 2014.

[13] M. Hagen, E. Quiroga-González, S. Dörfler, G. Fahrer, J. Tübke, M. J. Hoffmann*, et al.*, "Studies on preventing Li dendrite formation in Li–S batteries by using pre-lithiated Si microwire anodes," *Journal of Power Sources,* vol. 248, pp. 1058-1066, 2014.

[14] S.-K. Lee, S.-M. Oh, E. Park, B. Scrosati, J. Hassoun, M.-S. Park*, et al.*, "Highly Cyclable Lithium–Sulfur Batteries with a Dual-Type Sulfur Cathode and a Lithiated Si/SiOx Nanosphere Anode," *Nano Letters,* vol. 15, pp. 2863-2868, 2015.

[15] N. Moreno, M. Agostini, A. Caballero, J. Morales, and J. Hassoun, "A long-life lithium ion sulfur battery exploiting high performance electrodes," *Chemical Communications,* vol. 51, pp. 14540-14542, 2015.

[16] Y. Yamada and A. Yamada, "Review—Superconcentrated Electrolytes for Lithium Batteries," *Journal of The Electrochemical Society,* vol. 162, pp. A2406-A2423, 2015.

[17] L. Suo, Y.-S. Hu, H. Li, M. Armand, and L. Chen, "A new class of Solvent-in-Salt electrolyte for high-energy rechargeable metallic lithium batteries," *Nature Communications,* vol. 4, p. 1481, 2013.

[18] E. S. Shin, K. Kim, S. H. Oh, and W. I. Cho, "Polysulfide dissolution control: the common ion effect," *Chemical Communications,* vol. 49, pp. 2004-2006, 2013.

[19] R. Miao, J. Yang, X. Feng, H. Jia, J. Wang, and Y. Nuli, "Novel dual-salts electrolyte solution for dendrite-free lithium-metal based rechargeable batteries with high cycle reversibility," *Journal of Power Sources,* vol. 271, pp. 291-297, 2014.

[20] J. Hu, G. Long, S. Liu, G. Li, and X. Gao, "A LiFSI–LiTFSI binary-salt electrolyte to achieve high capacity and cycle stability for a Li–S battery," *Chemical Communications,* vol. 50, pp. 14647-14650, 2014.

[21] H. Kim, F. Wu, J. T. Lee, N. Nitta, H. T. Lin, M. Oschatz*, et al.*, "In Situ Formation of Protective Coatings on Sulfur Cathodes in Lithium Batteries with LiFSI-Based Organic Electrolytes," *Advanced Energy Materials,* vol. 5, p. 1401792, 2015.

[22] Y. Fu and A. Manthiram, "Silicon nanoparticles supported on graphitic carbon paper as a hybrid anode for Li-ion batteries," *Nano Energy,* vol. 2, pp. 1107-1112, 11// 2013.

[23] J. Gao, M. A. Lowe, Y. Kiya, and H. D. Abruña, "Effects of Liquid Electrolytes on the Charge–Discharge Performance of Rechargeable Lithium/Sulfur Batteries: Electrochemical and in-Situ X-ray Absorption Spectroscopic Studies," *The Journal of Physical Chemistry C,* vol. 115, pp. 25132-25137, 2011.

[24] Z. Jiang, M. Alamgir, and K. M. Abraham, "The Electrochemical Intercalation of Li into Graphite in Li/Polymer Electrolyte/Graphite Cells," *Journal of The Electrochemical Society,* vol. 142, pp. 333-340, 1995.

[25] A. Bhargav and Y. Fu, "Lithium Peroxide-Carbon Composite Cathode for Closed System Li-O2 Batteries," *Journal of The Electrochemical Society,* vol. 162, pp. A1327-A1333, 2015.

[26] Y. Fu, Y.-S. Su, and A. Manthiram, "Highly Reversible Lithium/Dissolved Polysulfide Batteries with Carbon Nanotube Electrodes," *Angewandte Chemie International Edition,* vol. 52, pp. 6930-6935, 2013.

[27] L. Qie, C. Zu, and A. Manthiram, "A High Energy Lithium-Sulfur Battery with Ultrahigh-Loading Lithium Polysulfide Cathode and its Failure Mechanism," *Advanced Energy Materials,* p. 1502459, 2016.

[28] J. Yang, J. Xie, X. Zhou, Y. Zou, J. Tang, S. Wang*, et al.*, "Functionalized N-Doped Porous Carbon Nanofiber Webs for a Lithium–Sulfur Battery with High Capacity and Rate Performance," *The Journal of Physical Chemistry C,* vol. 118, pp. 1800-1807, 2014.

[29] Y. Cui and Y. Fu, "Enhanced Cyclability of Li/Polysulfide Batteries by a Polymer-Modified Carbon Paper Current Collector," *ACS Applied Materials & Interfaces,* vol. 7, pp. 20369-20376, 2015.

[30] H. Wang, Y. Yang, Y. Liang, J. T. Robinson, Y. Li, A. Jackson*, et al.*, "Graphene-Wrapped Sulfur Particles as a Rechargeable Lithium–Sulfur Battery Cathode Material with High Capacity and Cycling Stability," *Nano Letters,* vol. 11, pp. 2644-2647, 2011.

[31] X. Ji, K. T. Lee, and L. F. Nazar, "A highly ordered nanostructured carbon-sulphur cathode for lithium-sulphur batteries," *Nature Materials,* vol. 8, pp. 500-506, 2009.

[32] Q. Pang, D. Kundu, and L. F. Nazar, "A graphene-like metallic cathode host for long-life and high-loading lithium-sulfur batteries," *Materials Horizons,* vol. 3, pp. 130-136, 2016.

[33] M. Wu, Y. Cui, and Y. Fu, "Li2S Nanocrystals Confined in Free-Standing Carbon Paper for High Performance Lithium–Sulfur Batteries," *ACS Applied Materials & Interfaces,* vol. 7, pp. 21479-21486, 2015.

[34] A. Bhargav, M. Wu and Y. Fu, "A Graphite-Polysulfide Full Cell with DME-Based Electrolyte," *Submitted manuscript,* April 2016.

5. SUMMARY

The works on lithium-oxygen batteries presented in this thesis introduces the concept of closed system lithium oxygen batteries. These batteries show good rechargeability and though the utilization of controlled material synthesis and encapsulation, better performance can be obtained. Material characterization clearly points to complete reversibility of the lithium peroxide decomposition and formation. Cells with up to 50 cycles while using charge capacity control protocol has been demonstrated.

The work on lithium-sulfur batteries utilizes a novel solid polysulfide deposition technique to incorporate sulfur into the cathode. A new electrolyte compatible with both sulfur and graphite anode is presented. Satisfactory full cell performance is also demonstrated.

6. RECOMMENDATIONS

Closed system lithium-oxygen clearly enables the functioning of the cell without the external supply of oxygen. This system could be to understand the reaction kinetics, electrolyte-cathode interaction, and parasitic reactions. It can also be used to study the use of oxygen storage materials, different electrolytes and non-Li anodes in such batteries.

Clear performance improvement is observed when lithium peroxide is chemically synthesized. The demonstrated synthesis technique can be utilized to control the size and morphology of lithium peroxide that forms the starting material. This method of cathode preparation can be used to develop cathodes with advanced carbonaceous and non-carbonaceous materials to enhance performance and prolong cycle life. Also, Li-metal free cells can be developed. These would enable long-life and safe Li-O_2 batteries in the future.

Lithium-sulfur batteries with the demonstrated polysulfide encapsulation technique can be used in ordered cathodes which can efficiently retain polysulfides thus minimizing the shuttle effect leading to prolonged cycle life of full cells. The new electrolyte can also be used with further optimized anodes having less porosity and higher capacities enabling high energy density lithium-sulfur batteries.